

FINAL REPORT

Title: High Spectral Resolution Infrared and Raman Lidar Observations for the ARM Program: Clear and Cloudy Sky Applications

For the period of: 1 November 1996 to 31 October 2008

Submitted to: The Department of Energy

Grant Number: DE-FG02-90ER61057

Date Submitted: 17 June 2009

UW Madison Project Number: 144GC22

Submitted by:
Space Science and Engineering Center
at the University of Wisconsin Madison
1225 West Dayton Street
Madison, WI 53706

Principle Investigator: Henry E. Revercomb, (608) 263-6758

**High Spectral Resolution Infrared and Raman Lidar Observations for the ARM
Program:
Clear and Cloudy Sky Applications**

Contents

1. Summary of Major Accomplishments for ARM	P 2
2. Cirrus Cloud Characterization using Raman Lidar and Radar	P 5
3. Clear Sky Radiative Closure Studies	P10
4. Scanning HIS: Airborne AERI for the ARM-UAV Program	P19
5. Cloud Studies	P22
5.1. Cloud Property Retrievals from AERI and Scanning HIS	P23
5.2. Cloud Radiative Transfer Closure Study at the ARM NSA Site	P28
5.3. AIRS Cloud Property Retrievals	P33
6. AERI Science Quality Assessment	P37
7. References and Bibliography	P38

Introduction

This grant to the University of Wisconsin-Madison with Dr. Hank Revercomb as PI has made key contributions to the ARM Program since its beginning in the early 1990's. Throughout this long commitment to the ARM program, we have successfully applied the expertise of our group in high spectral resolution infrared observing to the evolving and maturing needs of the overall ARM Program. As the clear sky objectives of the program have approached reasonable closure, we have turned our primary attention toward an emphasis on the all sky problem and the issue of characterizing larger scale properties for model applications.

In this summary of past accomplishments we have chosen to emphasize how our work from the most recent funding cycles have prepared us for the next 3-year effort. Section 1 contains a short summary of our major accomplishments for the ARM program. The other sections of this document describe our work with (Section 2) accurate cirrus cloud

characterization using combined Raman Lidar and cloud radar observations at the SGP site, (Section 3) clear sky radiative closure studies related to BBHRP, (Section 4) the Scanning High-resolution Interferometer Sounder (Scanning-HIS) aircraft instrument to provide the AERI-like view from above for the ARM UAV program, (Section 5) cloud retrieval algorithms for observations from AERI, Scanning-HIS during M-PACE, and the NASA Atmospheric IR Sounder (AIRS), and (Section 6) AERI data science quality assessment. The progress achieved with the SGP Raman Lidar data and with the high resolution spectra from AIRS, which has been made possible by our long term involvement with AIRS through the NASA AIRS Science Team and with support from NOAA, is key to our proposed cloudy radiative transfer closure and climate model assessment efforts.

The most recent work related to the proposed work has been prepared for submission for publication. These two papers (Borg et al. 2008b and Moy et al. 2008b), summarized in sections 2 and 3, represent significant progress achieved under the current ARM funding and will be formally submitted by the end of this summer.

1. Summary of Major Accomplishments for ARM

This grant began with the development of the Atmospheric Emitted Radiance Interferometer (AERI) for ARM. The AERI has provided highly accurate and reliable observations of downwelling spectral radiance (Knuteson et al. 2004a, 2004b) for application to radiative transfer, remote sensing of boundary layer temperature and water vapor, and cloud characterization. One of the major contributions of the ARM program has been its success in improving radiation calculation capabilities for models and remote sensing that evolved from the multi-year, clear-sky spectral radiance comparisons between AERI radiances and line-by-line calculations (Turner et al. 2004). This effort also spurred us to play a central role in improving

the accuracy of water vapor measurements, again helping ARM lead the way in the community (Turner et al. 2003a, Revercomb et al. 2003).

In order to add high-altitude downlooking AERI-like observations over the ARM sites, we began the development of an airborne AERI instrument that has become known as the Scanning High-resolution Interferometer Sounder (Scanning-HIS). This instrument has become an integral part of the ARM Unmanned Aerospace Vehicle (ARM-UAV) program. It provides both a cross-track mapping view of the earth and an uplooking view from the 12-15 km altitude of the Scaled Composites Proteus aircraft when flown over the ARM sites for IOPs. It has successfully participated in the first two legs of the “grand tour” of the ARM sites (SGP and NSA), resulting in a very good comparison with AIRS observations in 2002 and in an especially interesting data set from the arctic during the Mixed-Phase Cloud Experiment (M-PACE) in 2004.

More specifically, our major achievements for ARM include

1. Development of the Atmospheric Emitted Radiance Interferometer (AERI) to function like a satellite on the ground for ARM, providing a steady stream of accurately calibrated spectral radiances for Science Team clear sky and cloud applications (Knuteson et al. 2004a),
2. Detailed radiometric calibration and characterization of AERI radiances, with uncertainty estimates established from complete error analyses and proven by inter-comparison tests (Knuteson et al. 2004b),
3. AERI data quality assessment and maintenance over the extended time frames needed to support ARM (Dedecker et al., 2005)

4. Key role in the radiative transfer model improvements from the AERI/LBLRTM QME (Turner et al. 2004) and AERI-ER especially from the SHEBA experiment (Tobin et al. 1999),
5. Contributed scientific and programmatic leadership leading to significant water vapor accuracy improvements and uncertainty assessments for the low to mid troposphere (Turner et al. 2003a, Revercomb et al. 2003),
6. Leadership of the ARM assessment of the accuracy of water vapor observations from radiosondes, Raman Lidar and in situ aircraft observations in the upper troposphere and lower stratosphere (Tobin et al. 2002, Ferrare et al. 2004),
7. New techniques for characterizing clouds from AERI (DeSlover et al. 1999, Turner 2003b, Turner et al. 2003b),
8. Initial design and development of the Scanning-HIS aircraft instrument and application to ARM UAV Program missions (Revercomb et al. 2005), and
9. Coordinated efforts leading to the use of ARM observations as a key validation tool for the high resolution Atmospheric IR Sounder on the NASA Aqua platform (Tobin et al. 2005a)
10. Performed ARM site and global clear sky radiative closure studies that shows closure of top-of-atmosphere flux at the level of $\sim 1 \text{ W/m}^2$ (Moy et al 2008 and Section 3 of this appendix)
11. Performed studies to characterize SGP site cirrus cloud property retrievals and assess impacts on computed fluxes and heating rate profiles (Borg et al. 2008 and Section 2 of this appendix).

2. Cirrus Cloud Characterization using Raman Lidar and Radar

Cloud feedbacks represent the largest source of uncertainty in understanding climate sensitivity (IPCC, 2007). In order to address this uncertainty, to improve climate models, and to understand these feedbacks, improved measurements and characterizations of cloud properties are needed. In particular, the representation of cirrus clouds in models continues to be a significant problem. It is estimated that cirrus clouds cover between 20-35% of the Earth. This type of cloud plays a significant role in the energy budget of the atmosphere, but the magnitude and direction of the radiative forcing is dependent upon the cloud microphysical and macrophysical properties. Accurate and long-term measurements of cirrus cloud properties are needed. However, traditionally these measurements have proven difficult both for ground and satellite based instruments. This study provided a unique opportunity for measurement of cirrus cloud properties through the combined use of the Raman lidar and MMCR systems located at the ARM SGP site.

In this study, vertical profiles of cloud extinction were derived from the SGP Raman lidar system for uniform cirrus cases at SGP. These profiles were combined with data from the MMCR to produce a merged dataset on the same temporal and spatial resolution. The merged dataset is produced on a 5-minute interval, at a 300m vertical resolution between 6 -16 km, and begins in mid September 2004 (when the Raman lidar system was upgraded) and runs through the end of 2007. This 3 plus year record of cirrus cloud events at SGP combines the best of both systems; the ability of the Raman system to detect optically thin cirrus that the MMCR frequently misses, the ability of the MMCR to characterize optically thicker cirrus clouds that could saturate the lidar, and the combination of both for direct measurement of particle size where there is coincident data

This merged dataset was then used to derive cirrus cloud microphysical properties. For those cases when only the radar data was available, the radar Microbase logic was used to derive cloud properties as is done within BBHRP. This logic assumes that reflectivity and ice water content are related through a power law relationship and that effective radius is a simple function of temperature. When only lidar data was available, the lidar extinction was used with an assumed small effective radius. And for

those cases when both radar and lidar data were available simultaneously, direct measurements of extinction and particle size were used following the work by Donovan et al. (2001a, 2001b) with an assumed ice habit of hexagonal columns. These cirrus cloud microphysical properties were used with an assumed Ebert and Curry parameterization (Ebert and Curry, 1992) in RRTM along with atmospheric profile information from balloon sondes and microwave radiometers and surface information from radiation stations to compute infrared radiative TOA fluxes and heating rate profiles. These fluxes were compared with observations from the CERES and GOES platforms.

A single layer high altitude cirrus case from November 2005 is shown in Figure 1. Measurements from both the MMCR radar and Raman lidar are shown in Figure 1(a) with radar reflectivity in color and lidar derived cloud boundaries in black. In general, the radar is missing significant portions of the uppermost part of the cirrus cloud. Regions also exist where the radar is seeing more of the lower cloud layers, see 08:00 - 11:00 UTC on 11/09/2005 and 00:00 – 03:00 UTC on 11/10/2005, and where there is coincident radar and lidar data. Using only the information from the MMCR radar, heating rates are calculated using RRTM with the BBHRP Microbase logic, and profiles are shown in Figure 1(b). In those regions where there is significant radar reflectivity there is also significant heating (red) and cooling (blue). Heating towards cloud base and cooling towards cloud top. Adding the Raman lidar information to the radar gives RRTM computed heating rates as shown in Figure 1(c). The additional information results in more pronounced heating and cooling throughout the case study, especially evident during the second half of the study period. The resulting TOA fluxes are shown separately in Figure 1(d) and as a flux difference (radar-only minus the combined radar-lidar) in Figure 1(e). The regions with very thin cirrus clouds, see 09:00 and 21:00 UTC on 11/10/2005, that were missed by the radar, result in TOA flux differences on the order of -25W/m^2 . Although there are much larger flux differences in this study period, these types of very thin cirrus are typical of those missed by the radar and contribute significantly to the TOA fluxes and heating rates.

Many such study periods can be found within the longer 3-year dataset, but a question remains. How representative is this study period to the longer dataset? After accounting for known time periods

when the MMCR was problematic (eliminating all of 2007) and looking at those cases when the lidar is not attenuated, the resulting picture emerges. See Figure 2 which depicts a two-dimensional histogram of the lidar optical depth versus the optical depth fraction sensed by the radar with the colorscale representing the number of observations. For lidar optical depths less than 1, the MMCR frequently does not detect a significant fraction of the cloud optical depth. Even for cloud optical depths greater than 1, the MMCR sees only approximately 80% of the cloud optical depth. Combined with the flux and heating rate errors associated with these types of cloud optical depth differences, this is an important finding and one which will have significant impacts on the use of ARM cloud products for radiative closure and climate model parameterization studies. Other specific outcomes and conclusions from this study are:

- Derived extinction algorithm for Raman lidar system at SGP.
- Produced preliminary 3 year merged dataset of Raman lidar and MMCR data.
- Using cloud radar data alone can miss significant upper level cirrus resulting in large errors in computed fluxes and heating rates.
- The accurate characterization of thin cirrus can be achieved with a) Raman lidar extinction plus radar or b) AERI plus lidar cloud boundaries.
- The vertical distribution of extinction and particle size are significantly less important than optical depth in computing heating rates.

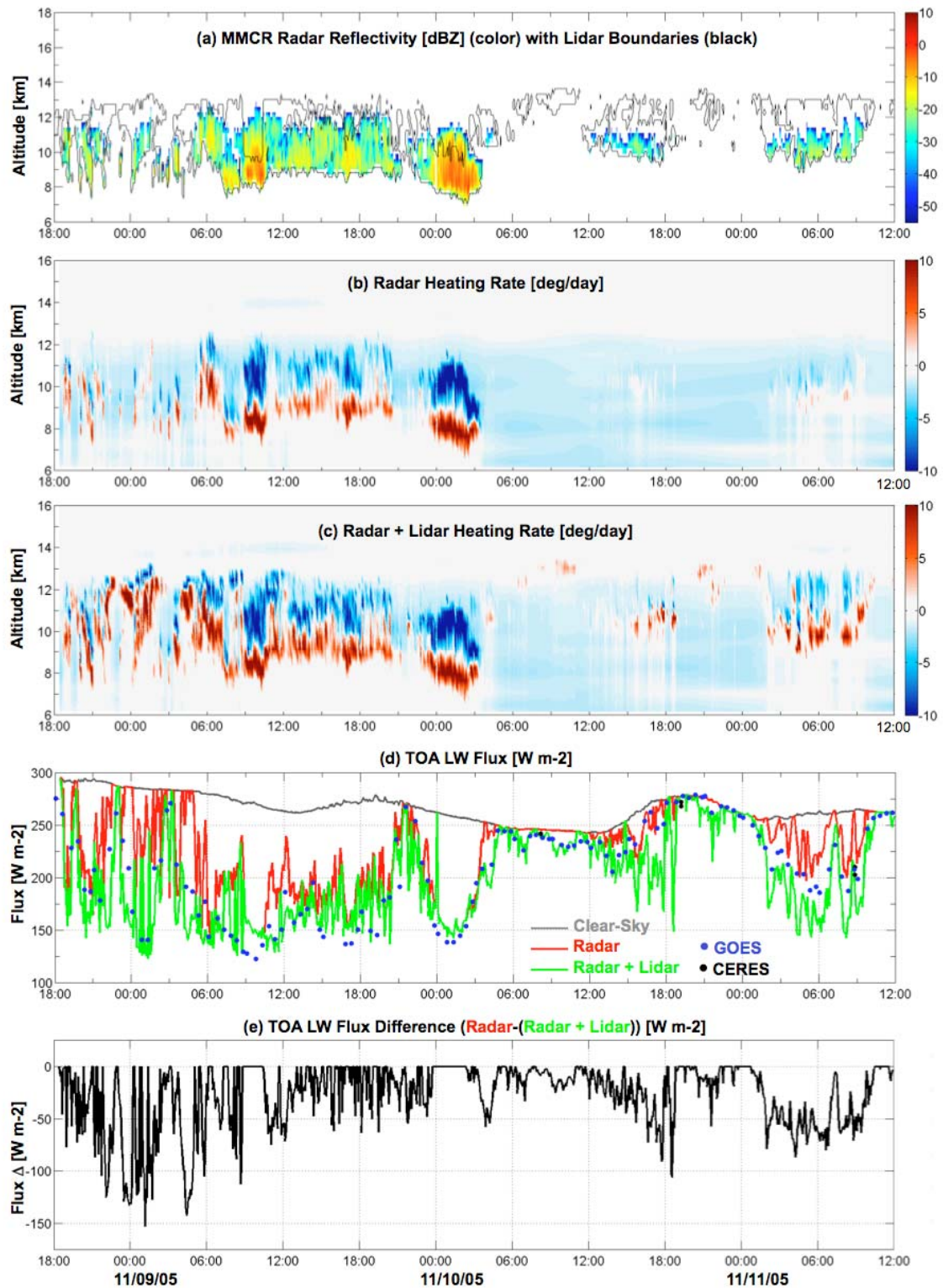


Figure 1. SGP Cirrus Cloud Case Study. Refer to the text beginning on page P6.

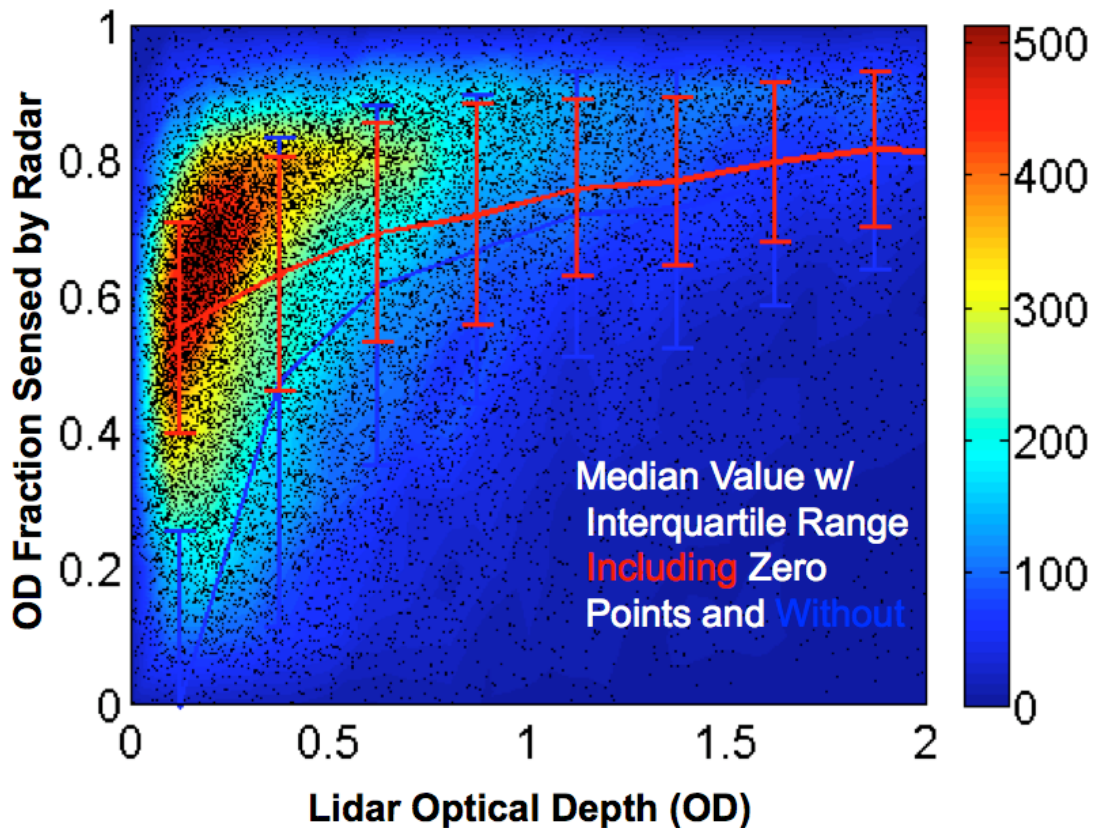


Figure 2. Histogram of lidar optical depth versus optical depth fraction sensed by radar for those cases when lidar NOT attenuated, 09/17/2004-12/31/2006. The figure does not include samples for when the Raman lidar sees a cloud but the cloud radar does not. See the text starting on page P6.

3. Clear Sky Radiative Closure Studies

The earth's radiant energy budget is a balance between absorbed solar radiation and emitted outgoing longwave radiation (OLR). For almost 50 years now, accurate, long term records of solar insolation, planetary albedo, and OLR have been collected to monitor climate change. This section describes results of two closure studies: one tests how well a state of the art radiative model using satellite retrievals from Atmospheric Infrared Sounder (AIRS) reproduces clear sky observations of OLR obtained by the Clouds and the Earth's Radiant Energy System (CERES) broadband radiometer, and the other tests how well the AIRS retrievals input into the radiative model reproduces AIRS radiances. In both studies

the methodologies were tested at the Department of Energy (DOE) Atmospheric Radiation Measurement (ARM) program site in the U.S. Southern Great Plains (SGP) where we have a long history and familiarity with the validation data sets. The methods are then applied globally. The clear sky OLR comparisons were impressive; RRTM calculations agree with CERES observations to $\sim 1 \text{ W/m}^2$ with an uncertainty of $\sim 1 \text{ W/m}^2$ at SGP between September 2002 and February 2005 and globally (with some *understood* regional exceptions) for four study days. Global analyses as a function of the International Geosphere Biosphere Programme (IGBP) surface types quantified clear sky OLR agreements for exceptionally bad (desert and snow/ice) and good (ocean) regions. AIRS spectral analysis uncovered a persistent bias in the upper level water vapor reported by AIRS retrievals but no day/night bias necessary to explain the day/night bias seen in the OLR comparisons to CERES. We were also able to offer one of the few, albeit tentative, estimates of the error in the far infrared (a radiatively important but understudied spectral region) to be better than $\sim 0.3\%$ for clear skies. Extending the ARM SGP results to the global scale demonstrates the new capacity of observed spectrally resolved radiances that convey higher information content than CERES-type instruments with no substantial corrosion in accuracy.

We used the line-by-line radiative transfer model (LBLRTM), developed under the DOE ARM program, to provide computations of top of atmosphere radiances (Clough et al. 2005). The line parameter database and code base adopted for LBLRTM has been validated using University of Wisconsin High-resolution Interferometer Sounder (HIS) and scanning HIS aircraft observations at high altitude over the past 20 years (Clough et al. 2005; Revercomb et al. 2003). A series of ground-based closure experiments has also been conducted over the past 10 years at the DOE ARM sites evaluating both the model inputs (e.g. atmospheric state) and the comparison to University of Wisconsin Atmospheric Emitted Radiance Interferometer (AERI) downwelling radiances (Knuteson et al. 2004; Revercomb et al. 2003; Turner et al. 2004). The Atmospheric and Environmental Research (AER), Inc. has developed the rapid radiative transfer model (RRTM) which uses a correlated-k method for radiative transfer based on prior

calculations using LBLRTM (Clough et al. 2005). The RRTM was used to calculate shortwave fluxes, longwave fluxes and cooling rates at any level in 16 wavebands.

Our study compared calculations to CERES Single Scanner Footprint TOA/Surface Fluxes and Clouds (SSF) product CER_SSF_Aqua-FM3-MODIS_Edition 2B which contains one hour of instantaneous OLR data (Geier et al. 2003). Each CERES instrument has three channels - a shortwave (SW) channel (0.2-5 μm) to measure reflected sunlight, a 8-12 μm "window" region (WN) channel to measure Earth-emitted thermal radiation, and the total channel (0.2-100 μm) to measure all wavelengths of radiation. CERES OLR is estimated as the total minus the shortwave radiation, which is a potential source of day/night bias (Minnis and Khaiyer 2000; Minnis, Gambheer and Doelling 2004).

In order to cover a wide range of atmospheric conditions, comparisons were made at the ARM SGP site for almost 2.5 years with both in-situ ARM measurements and retrievals from AIRS used as inputs for the RRTM calculations. As a part of ongoing AIRS Science Team efforts and a collaborative effort between the NASA Earth Observing System (EOS) project and the DOE ARM program, data from various ARM and other observations were used to create best estimates of the atmospheric state at the Aqua overpass times. The resulting Best Estimate (BE) profile validation data set is an ensemble of temperature and water vapor profiles based on radiosondes and other site and satellite based instruments, interpolated to the Aqua overpass time (Tobin et al. 2006). AIRS is the first of a new generation of satellite-based advanced infrared sounders, and produces retrievals of temperatures and water vapor with high accuracy under clear and partly cloudy conditions (Aumann et al. 2003). Tobin et al. (2006) used the ARM site Best Estimate profiles to validate the AIRS Team temperature and water vapor retrievals for the tropical ocean site and the mid-latitude land SGP site for all sky conditions.

Both CERES comparisons with RRTM calculations using ARM data and with AIRS satellite retrievals had a remarkably small mean bias but also had an unexplained significant day/night bias. Table 1 lists the mean and standard deviations of the comparisons for day, night, and both day and night together.

OLR differences: Observations minus Calculations		Mean, W/m ²	Stdev, W/m ²	npts	Day-Nite Bias	Statistical uncertainty
CERES - ARM RRTM	Day	-0.2	4.6	53	-0.7	0.7
	Night	+0.5	2.6	74		
	D&N	+0.3	3.6	127		
CERES - AIRS* RRTM * Numbers reflect correction to upper level water vapor	Day	-0.5	2.7	53	-1.8	0.4
	Night	+1.2	1.8	74		
	D&N	+0.5	2.4	127		

Table 1: Clear sky OLR comparison at SGP. CERES minus RRTM calculation statistics for day, night, and combined day and night given.

The bias for all the comparisons is ~ 1 W/m² after a correction to the AIRS upper level water vapor was made based on AIRS spectral analysis. Daytime variability is almost twice that of nighttime variability in the CERES – ARM RRTM comparison (4.6 and 2.6 W/m²). The day/night bias is the same magnitude as the level of statistical uncertainty of 0.7 W/m². The CERES – AIRS RRTM has a statistically significant day/night bias of -1.8 W/m². For both comparisons the uncertainty in the mean is ~ 1 W/m², estimated from the statistical uncertainty and day/night bias.

AIRS spectral radiance analysis has the distinct advantage of allowing for a careful evaluation of the profiles; we found a positive $\sim 10\%$ upper level water bias (AIRS retrievals too wet above 5 km) in the AIRS retrievals. Figure 3 is a plot of observed AIRS brightness temperatures differences with LBLRTM calculations using AIRS retrievals for daytime (top panel) and night (bottom panel). The mean of the observed minus calculated differences is shown with error bars of one standard deviation for the 127 matched comparisons at SGP. The differences are less than 2 K with understood exceptions in the shortwave (greater than 2200 cm⁻¹) where LBLRTM does not account for non Local Thermodynamic Equilibrium and surface solar reflection in the daytime. More critically, the spectral range between ~ 1250 to 1614 cm⁻¹ (the vibrational 6.3 μm H₂O band) shows a ~ 0.6 K bias offset. There was no such bias in the ARM validation data set (not shown).

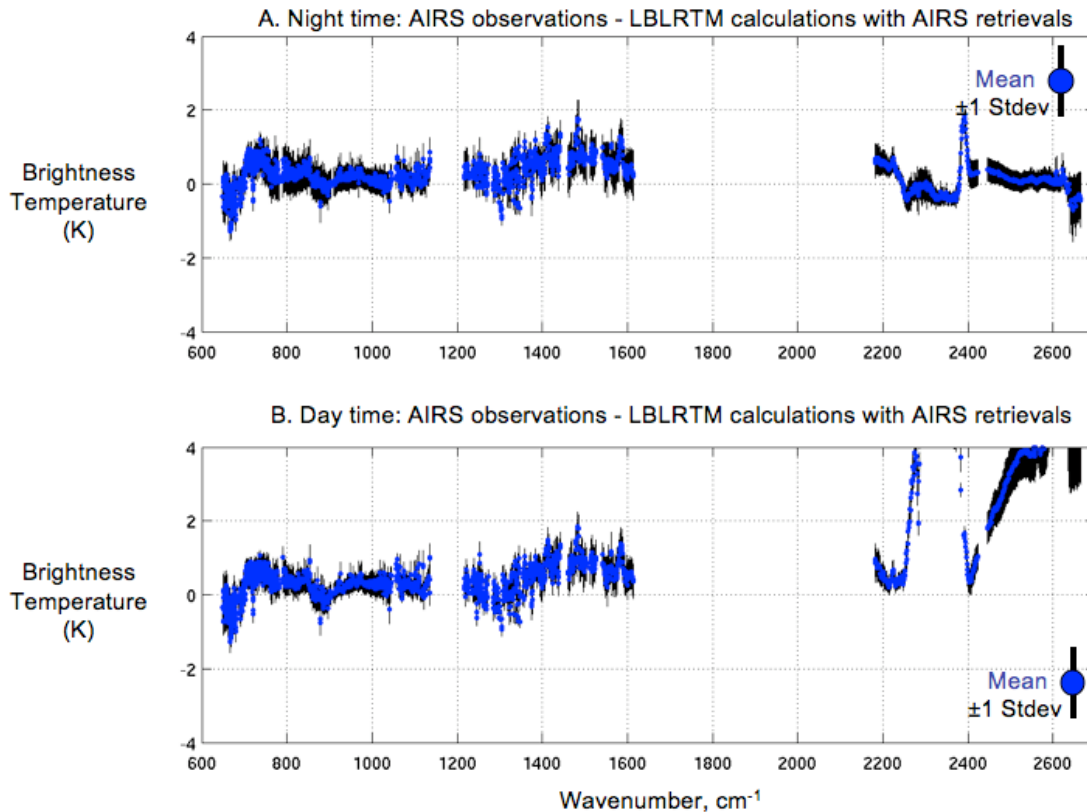


Figure 3: AIRS spectral radiance analysis. AIRS radiance observations minus LBLRTM radiance calculations based on AIRS retrievals. Top panel shows nighttime differences, bottom panel shows daytime differences.

AIRS spectral analysis also showed only minor differences between night and day (with known exceptions in the shortwave) which cannot account for the day/night bias seen in the CERES – RRTM OLR comparisons. CERES ADMs do not take into account variations in anisotropy with solar zenith angle and relative azimuth angle. This approximation works well for oceans and all surfaces at night, but it breaks down in the daytime for certain land types with highly variable topography (Loeb et al. 2005). The global study is presented with biases as a function of IGBP surface types and suggests that the day-night bias for ocean scenes is very small.

Direct estimations of the error in the far infrared (such as the ARM program’s closure experiments for the near infrared) are difficult because the atmosphere is opaque to the far infrared from

most ground-based observing stations and there are few spectrally resolved radiometers for the far infrared. But the far infrared spectral region is important; it is dominated by the pure water vapor rotation band which contributes strongly to atmospheric cooling of the upper troposphere. AIRS spectrally resolved radiances were converted into partial fluxes to calculate the percentage OLR error in the spectra covered by AIRS (~0.3%). Assuming CERES errors are similar throughout the entire spectrum, and that there are no cancellation of errors between CERES and RRTM, our new technique allows us to infer the error in the far infrared to be between 0.1 and 0.3%.

We extended the AIRS RRTM calculations globally for 16 November 2002, 18 February 2003, 5 May 2003, and 9 August 2003. Except for some regional differences the agreement between observations and calculations is remarkably good, generally within 2 W/m^2 and even better over the oceans. For a typical example Figure 4 is a map of differences for daytime on November 16, 2002. Large regional differences are apparent during the daytime in the desert regions including broad areas of the African Sahara, South African Kalahari and Australian deserts on the order of -20 W/m^2 (which is off the color scale). Not shown are differences greater than $+10 \text{ W/m}^2$ apparent during the nighttime in high latitude regions with persistent snow and ice cover (especially noticeable in Greenland). The latitudinal dependence of observed (CERES) and calculated (AIRS RRTM) OLR and OLR differences are shown for 16 November 2002 in Figure 5.

In general clear sky OLR is at a maximum near the equator and decreases towards the poles. Large exceptions are readily apparent and identified by region. At night the bias (Figure 4(a) bottom panel) is remarkably flat over the latitudes less than 60 degrees with an overall mean bias of 0.9 W/m^2 and standard deviation of 2.6 W/m^2 . In the higher latitudes there are large positive deviations on the order of $+10 \text{ W/m}^2$, which are comprised primarily of the region over Greenland. During the daytime (Figure 7(b) bottom panel), the bias has more variability, especially in the desert regions. The daytime overall mean bias for latitudes less than 60 degrees is -1.0 W/m^2 and the standard deviation is larger with respect to the daytime (5.6 W/m^2). During both day and night and over all latitudes, bias outliers are more numerous in the negative direction indicating either that observations are underestimating or calculations are

overestimating the OLR. These negative outliers are consistent with undetected clouds. Results for the other three study days are similar, but are not shown. Comparisons were also parsed as a function of IGBP surface type and showed the largest biases and day/night biases over deserts and permanent snow and ice (Table 2).

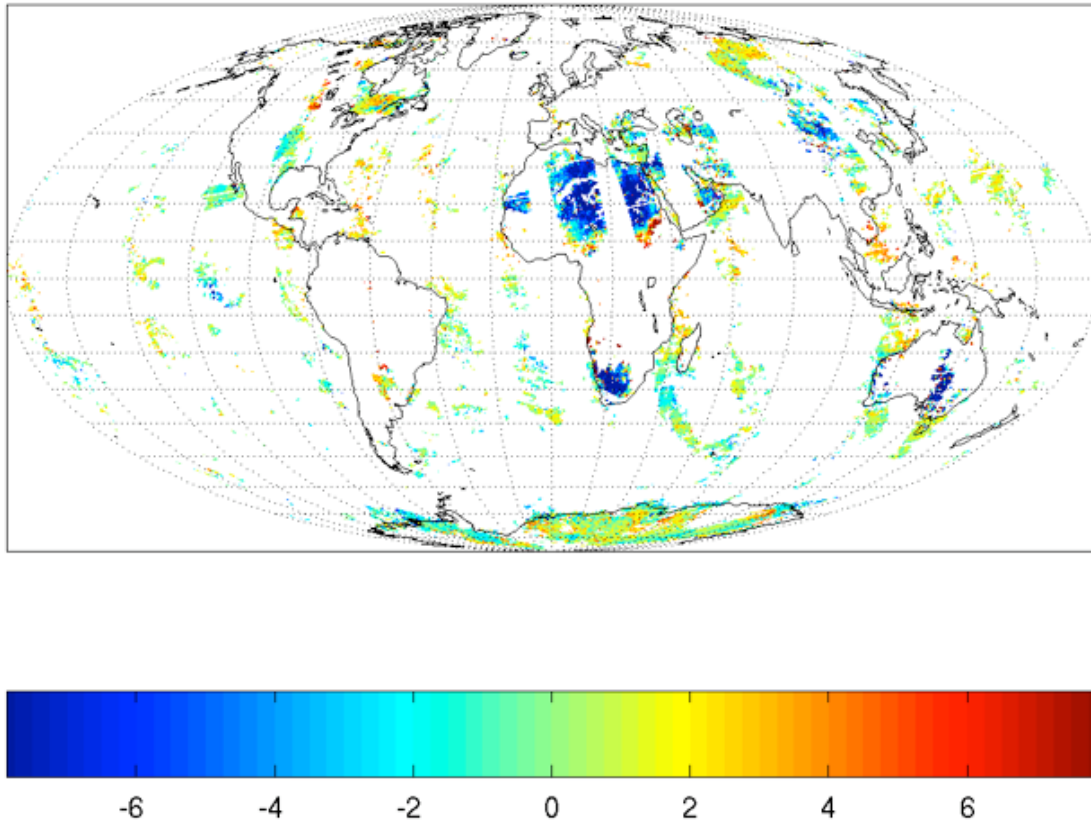


Figure 4: Map of clear sky OLR flux differences for daytime 16 November 2002, CERES minus AIRS RRTM. Color scale ranges from -7 to +7 W/m².

Most surface types (14 of 20) are slightly positively biased, and the remaining types (7,9,10,16,19,20) are slightly negatively biased. Only two surface types have biases greater in magnitude than 2 W/m², 15-Permanent Snow/Ice (+2.6 W/m²) and 16-Barren Rock and Desert (-3.4 W/m²). These are two surfaces with known problems in cloud identification and retrievals. As might be expected, 17-Water Bodies

(which is dominated by ocean scenes) has the largest number of points and one of the smallest biases (+0.2 W/m²) and standard deviations (1.9 W/m²).

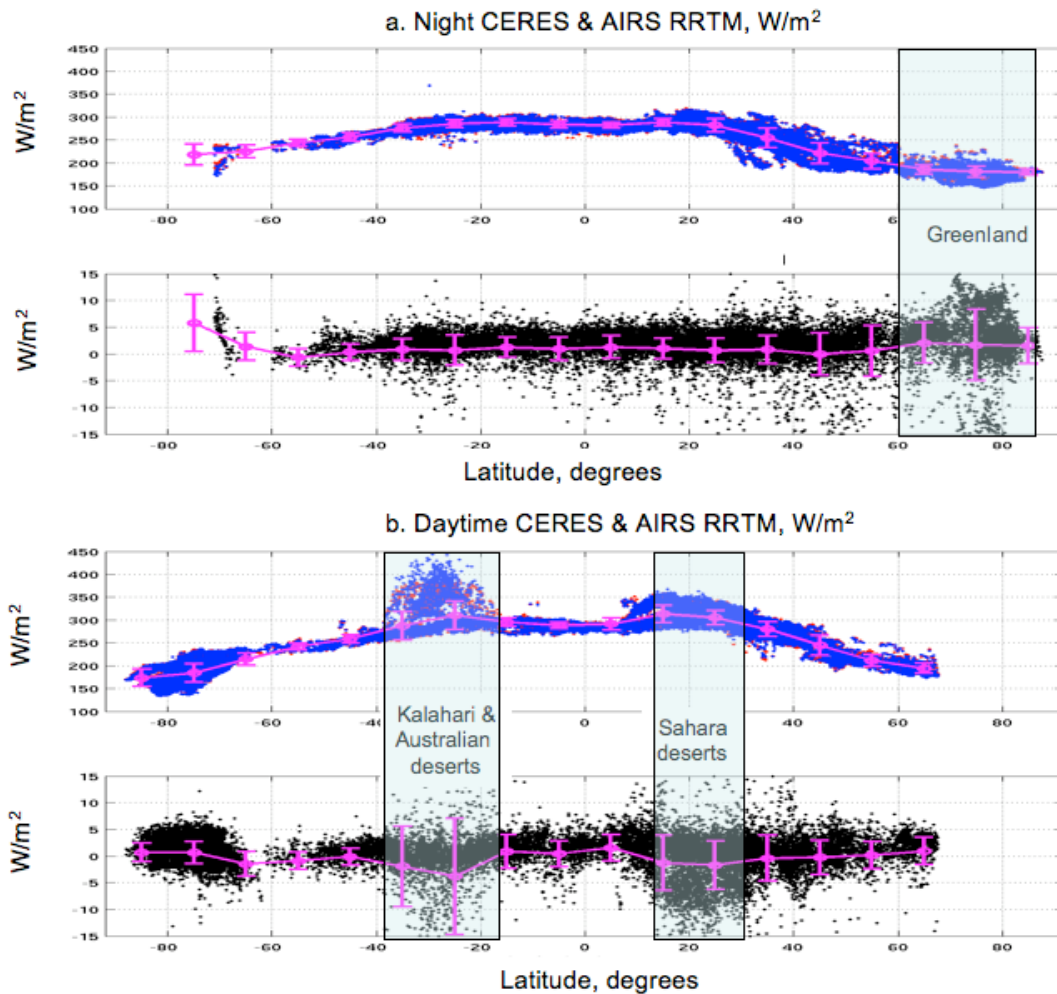


Figure 5: Latitude dependence of OLR for 16 November 2002. CERES points in red, AIRS RRTM points in blue. Top panels are clear sky OLR, and bottom panels are CERES – AIRS RRTM. Mean and 1 standard deviations shown in pink.

The nighttime scenes at latitudes less than 60 degrees is a subset which avoids the known problems of daytime desert and permanent snow and ice regions. The average biases for the subset for the four study days are: +0.9, +0.4, +0.4, and +0.4 W/m². Figure 6 is a histogram of CERES – AIRS RRTM OLR differences for November 16, 2002 (in blue) which has a mean of +0.9 and a standard deviation of 2.7 W/m². A Gaussian curve made to fit the differences (mean of 1.2 and standard deviation

of 1.5 W/m^2) is also drawn in red. The mean of the Gaussian curve is larger than the data by 0.4 W/m^2 and its standard deviation is smaller by 1.2 W/m^2 . Defining the statistical uncertainty as the standard deviation divided by the square root of the sample size, results in an uncertainty of 0.01 W/m^2 . Given the small statistical uncertainty, a conservative estimation of the total uncertainty is $\sim 0.4 \text{ W/m}^2$. The greater number of outliers on the negative side are consistent with undetected clouds in our sample. The total uncertainty in the mean for each of the three other study days is less than 0.4 W/m^2 . Our conclusion is that CERES – AIRS RRTM comparisons excluding known problems in the daytime and high latitude surfaces have a mean bias $\sim 1 \text{ W/m}^2$ with an estimated uncertainty of $\sim 0.4 \text{ W/m}^2$.

	Mean	Std Dev	Num points	Day-Night
1 Evergreen Needleleaf Forest	+1.1	2.5	255	+0.1
2 Evergreen Broadleaf Forest	+0.5	2.9	362	+1.4
3 Deciduous Needleleaf Forest	+0.4	2.1	35	-0.0
4 Deciduous Broadleaf Forest	+0.1	3.4	78	+0.7
5 Mixed Deciduous Forest	+0.7	2.8	249	+0.1
6 Closed Shrubland	+0.5	2.5	75	-0.7
7 Open Shrubland	-0.8	7.8	1,745	-5.2
8 Woody Savanna	+0.4	3.4	371	+0.8
9 Savanna	-0.2	5.7	830	-1.3
10 Grassland	-1.8	7.6	813	-4.2
11 Permanent Wetland	+1.9	1.0	15	-2.9
12 Cropland	+0.1	5.5	1,157	-1.9
13 Urban	-	-	0	-
14 Crop/Natural Veg. Mosaic	+0.4	3.2	855	-0.9
15 Permanent Snow/Ice	+2.6	3.8	6,951	-4.9
16 Barren/Desert	-3.4	8.1	4,071	-7.5
17 Water Bodies	+0.2	1.9	19,002	-0.5
18 Tundra	+1.9	5.6	34	-2.4
19 Fresh Snow	-1.7	2.7	2,739	-3.7
20 Sea Ice	-1.6	3.9	3,468	-0.7

Table 2: Clear sky OLR four day average comparison by IGBP surface type.

Extending the ARM SGP results to the global scale demonstrates the new capacity of observed spectrally resolved radiances that convey higher information content than CERES-type instruments with no loss of accuracy. Unlike broadband measurements of clear sky OLR, RRTM calculations using retrievals also provides clear sky heating rate profiles and fluxes throughout the atmosphere. But obtaining cloud conditions in the necessary form for RRTM calculations remains a formidable challenge. Our current proposal addresses these issues and lays out a plan for extending these analyses to cloudy sky conditions with a focus on cirrus clouds.

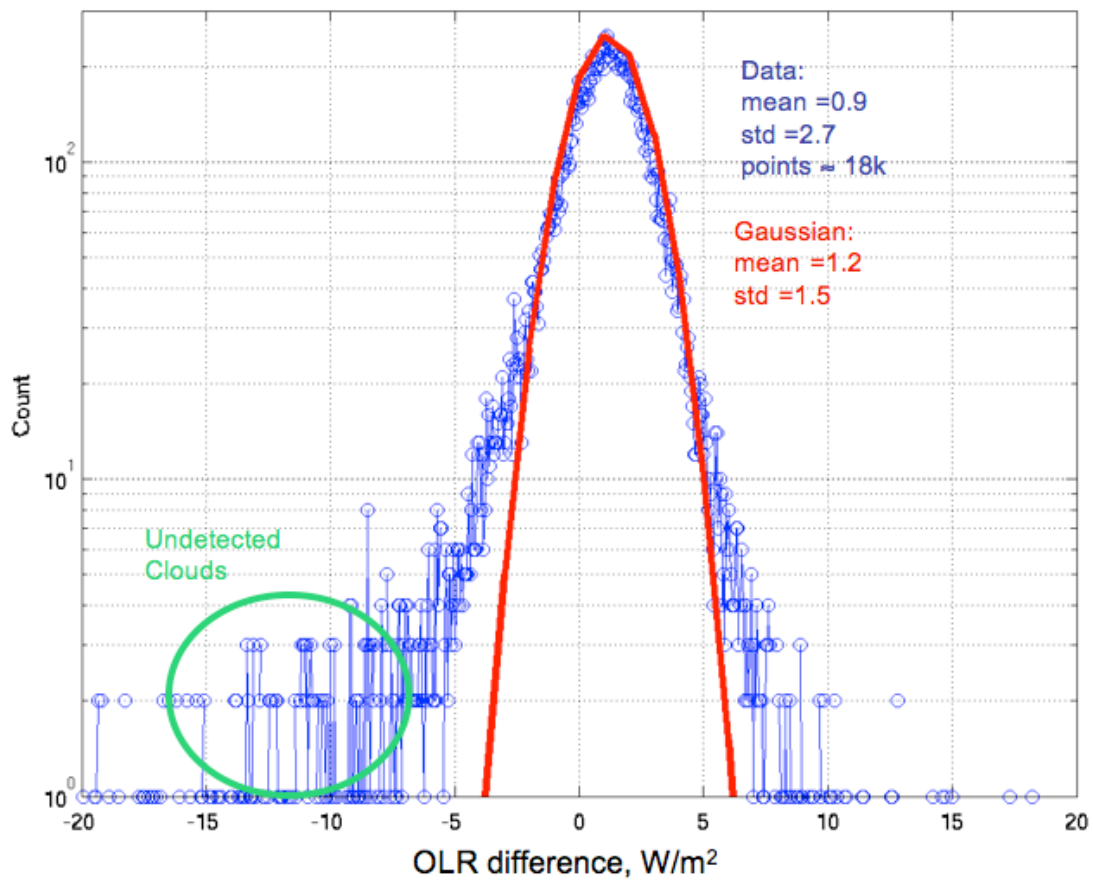


Figure 6: Histogram of CERES minus AIRS RRTM OLR differences for 16 November 2002. Nighttime and latitudes less than 60 degrees.

4. Scanning HIS: Airborne AERI for the ARM-UAV Program and the AIRS connection for space-based data

The Scanning-HIS is an aircraft sensor that provides accurate measurements of the upwelling infrared spectrum at similar spectral resolution and coverage to AERI (see Facilities and Resources appendix). Original development of the Scanning-HIS began in the mid 1990s with support of the ARM UAV program. With support from ARM, Integrated Program Office, and NASA, the Scanning-HIS has matured and is now an established tool for various applications including science process studies and satellite validation. A recent addition to its capabilities is the ability to collect zenith view data from flight altitude. The Scanning-HIS participated in the SGP and NSA components of the ARM-UAV “Grand Tour”. A summary of

Flight Date	Sortie #	Mission Summary	Start, End Time (UTC)	
10/08/2004	292	Barrow/Oliktok overpass	18:00	24:00
10/09/2004	293	Barrow/Oliktok overpass	19:00	00:40
10/10/2004	294	A-Train Under-flight SE of Fairbanks	21:15	23:15
10/12/2004	295	Barrow/Oliktok overpass	20:30	01:30
10/15/2004	296	A-Train Under-flight West of Fairbanks	21:30	24:00
10/17/2004	297	Barrow overpass and Cloud Sampling	19:30	01:30
10/18/2004	298	Oliktok overpass and Cloud Sampling	19:15	00:30

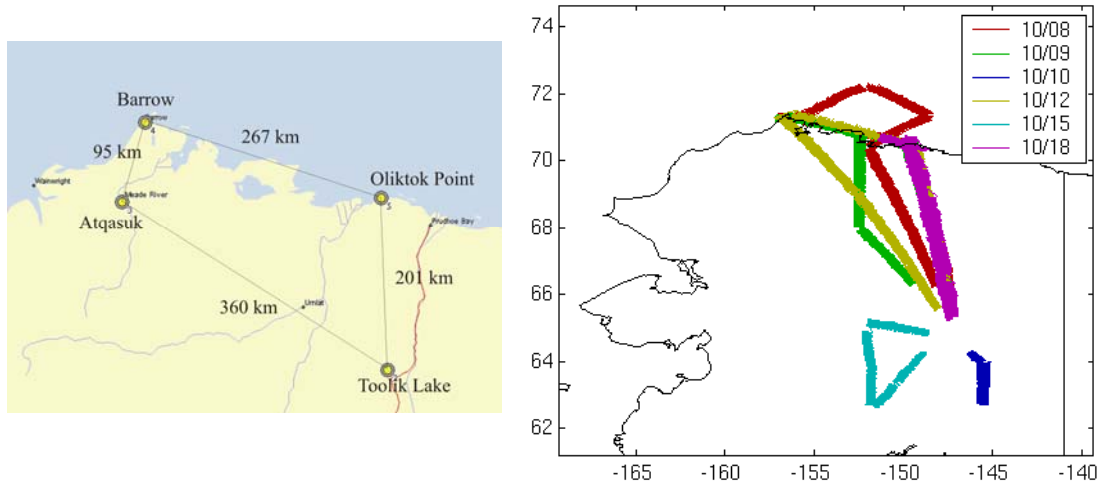


Figure 7. Scanning-HIS flight tracks for the M-PACE field campaign, conducted out of Fairbanks, Alaska. In addition to the primary ARM goals for M-PACE, the flights also provided underflights of EOS Aqua and Terra for cold scene radiance validation and overpasses of various ground truth sites for testing and improving cloud detection and retrieval algorithms. The data from all flights is of high quality.

Scanning-HIS flights during the recent Mixed Phase Arctic Cloud Experiment conducted out of Fairbanks, AK, is given in Figure 7. Scanning-HIS data collected during M-PACE are being used for various ARM studies, some of which are described in the following sections. An example case study from M-PACE is shown In Figure 8, where AERI measurements of the downwelling radiance at the ground and Scanning-HIS measurements of the upwelling and downwelling radiance within and above cirrus clouds on 17 October 2004 are being used in a closure study to assess our ability to measure cloud microphysical properties and to model cloud radiation.

High spectral resolution infrared observations are now also available from the Atmospheric Infrared Sounder (AIRS) on the NASA EOS Aqua polar orbiting satellite that gives full cross track coverage with 3 by 3 14 km footprints covering a 50 km square at nadir. Our AIRS science team efforts (investigators Revercomb, Tobin, and Knuteson are members of the current AIRS science team) have focused on validation of the AIRS spectral radiances, temperature and water vapor profile retrievals, and land surface fields. These efforts have demonstrated that AIRS observations are of very high quality and should be adopted for ARM applications. In particular, validation studies using Aqua underflights by the Scanning-HIS have shown that AIRS has very good absolute radiometric and spectral accuracy, with observed differences less than 0.2 K for the majority of spectral channels throughout the long, mid, and shortwave spectral regions (Tobin et al. 2005b). We have also performed validation of the AIRS temperature and water vapor retrievals using “best estimates” of the atmospheric state derived from various ARM data, including radiosondes launches at the Aqua over pass times, providing an accurate characterization of the AIRS retrieval products (Tobin et al. 2005b). In addition to these AIRS science team efforts, we have developed algorithms to retrieve temperature, water

vapor, surface, and cloud fields from the AIRS data, as described in Section 3.3. We are proposing to put these capabilities to use for ARM.

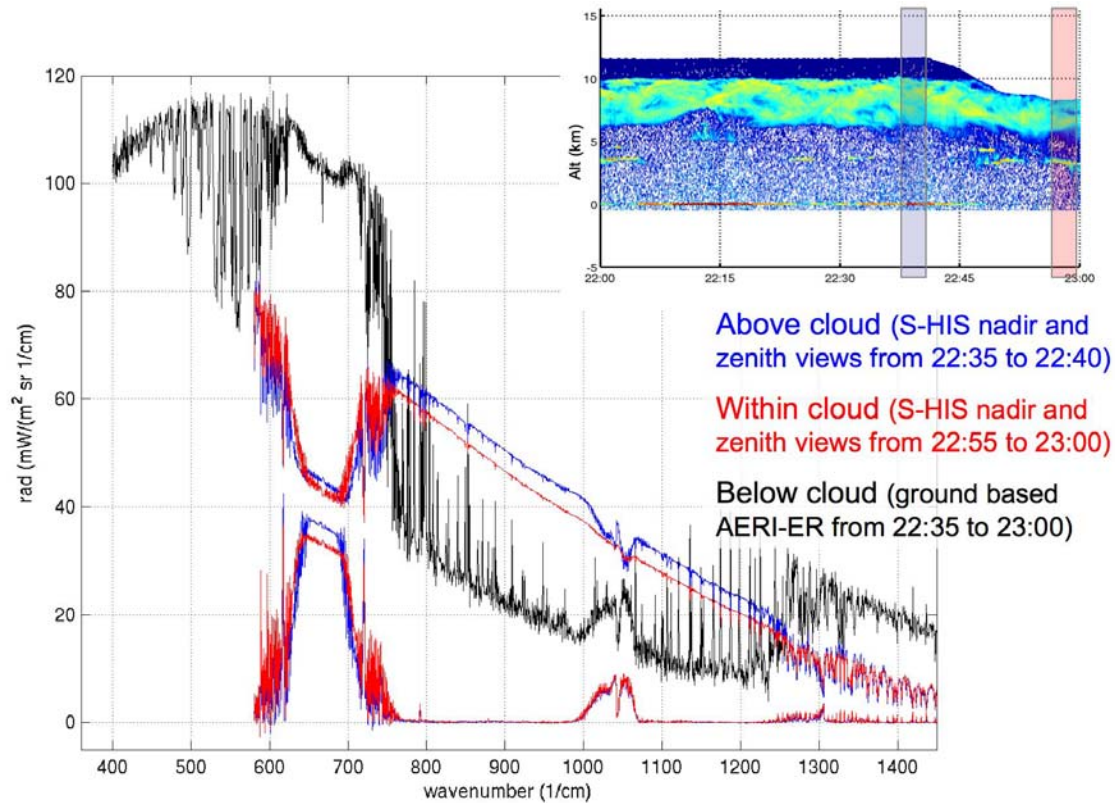


Figure 8. Ground-based AERI-ER and Scanning-HIS measurements (up and down from a 9 km flight altitude) at Barrow, AK on 17 October 2004 during the M-PACE experiment.

5. Cloud Studies

Under our current grant, we turned our expertise in the arena of high-spectral resolution infrared measurements to the topic of cloud remote sensing. High-spectral resolution infrared (HSR-IR) data have several advantages over the visible and near-infrared reflectance retrieval techniques utilized by the MODIS and GOES satellite instruments. In particular, HSR-IR data have a greater retrieval sensitivity to low optical thickness clouds (visible optical thickness less

than three) than reflectance-based retrievals. Also, HSR infrared data are effective for both day and night measurements, providing a distinct advantage in polar regions.

Our past ARM funding has allowed us to develop and demonstrate high-spectral resolution cloud optical property retrieval techniques for three platforms: the ground-based AERI, the aircraft-based Scanning-HIS, and satellite-based AIRS instruments. Over the ARM sites, ARM lidar and radar data are being used to evaluate these retrievals and to constrain the AERI and Scanning-HIS retrievals on a case-by-case basis. Cirrus cloud optical depth and effective radius are retrieved using similar techniques for both AERI and Scanning-HIS data, while a somewhat different approach is taken for ground-based AERI retrievals of mixed-phase clouds in the Arctic. A UW-Madison developed algorithm for the retrieval of cloud properties from AIRS radiances from the EOS Aqua platform has been applied to observations during the MPACE campaign. Results of these various approaches are described in the following subsections.

5.1. Cloud Property Retrievals from AERI and Scanning HIS

AERI measurements have been shown to provide the ability to infer cloud optical properties from both cirrus (Collard et al., 1995, DeSlover et al., 1999) and mixed-phase (Turner, 2005) clouds. A robust algorithm developed through our ARM funding by DeSlover combines AERI, lidar, and radiosonde measurements to retrieve cirrus optical depth (OD), and cloud effective radius. From these retrieved quantities, ice water path (IWP) and number density are inferred. Recent advancements in the AERI processing software allow rapid-sample measurement (Dedecker et al., 2005); which provides sub-minute sample periods, consistent with lidar measurements, and is conducive to the study of cloud properties. The retrieval algorithm

has been updated by inclusion of non-spherical ice crystal single-scattering properties (Yang et al., 2003).

The DeSlover AERI algorithm relies on AERI, ARM lidar, and ARM radiosonde data. Radiosonde data are used with a line-by-line radiative transfer model to calculate clear sky optical depths, below cloud base and above cloud top, as identified by ARM lidar measurements. A spectral cloud optical depth is calculated based on inversion of the radiative transfer calculation and comparison with AERI observations. The spectral variations in each optical depth measurement are used to infer cloud particle effective radius from a database of extinction calculations. Retrievals are made under the assumption of an ice crystal habit; current crystal habits are hexagonal columns, bullet rosettes, or spherical particles.

An example of the AERI retrievals are shown in Figure 9 for a cirrus case over the DOE ARM SGP Central Facility during the Texas 2002 (TX2002) field campaign. The SGP-CRF Raman lidar depolarization ratios (upper panel) show a cirrus cloud between 10 and 14 km from 0400 to 1100 UTC on 29 November 2002. In the middle panel, comparisons are made between Raman lidar measured optical depths (black line), AERI retrieved optical depths using the DeSlover algorithm (blue line), and satellite derived optical depths from the Eighth Geostationary Operational Environmental Satellite (GOES-8, black diamonds). There is a high level of consistency between the AERI and Raman lidar optical depths throughout the time period, even during the period of strong oscillation in optical depth between 0800 and 1000 UTC. The ability to retrieve these optical depth oscillations, due to the passage of a wave cloud, as confirmed with Whole Sky Imager data (not shown), is made possible by updated AERI rapid-sampling capabilities. As the oscillation period is on the order of 10 minutes, the features would have been lost with the previous AERI sample mode that had nominal 7 minute sampling. The

GOES-8 optical depth retrievals are performed using the visible infrared solar-infrared, split-window technique (VISST) and the solar-infrared infrared split-window technique (SIST) (Minnis et al., 2002). These optical depth retrievals are biased low relative to the AERI and Raman lidar retrievals. The AERI derived bulk effective radius (bottom panel) is determined to range between 15 and 20 μm for this case. Figure 3 illustrates that the new rapid sample AERI observations provide the detailed time sampling needed to characterize the cloud variability and that the DeSlover algorithm provides a robust method for the retrieval of cloud optical depths ($\text{OD} > 1$) as validated by the SGP Raman lidar.

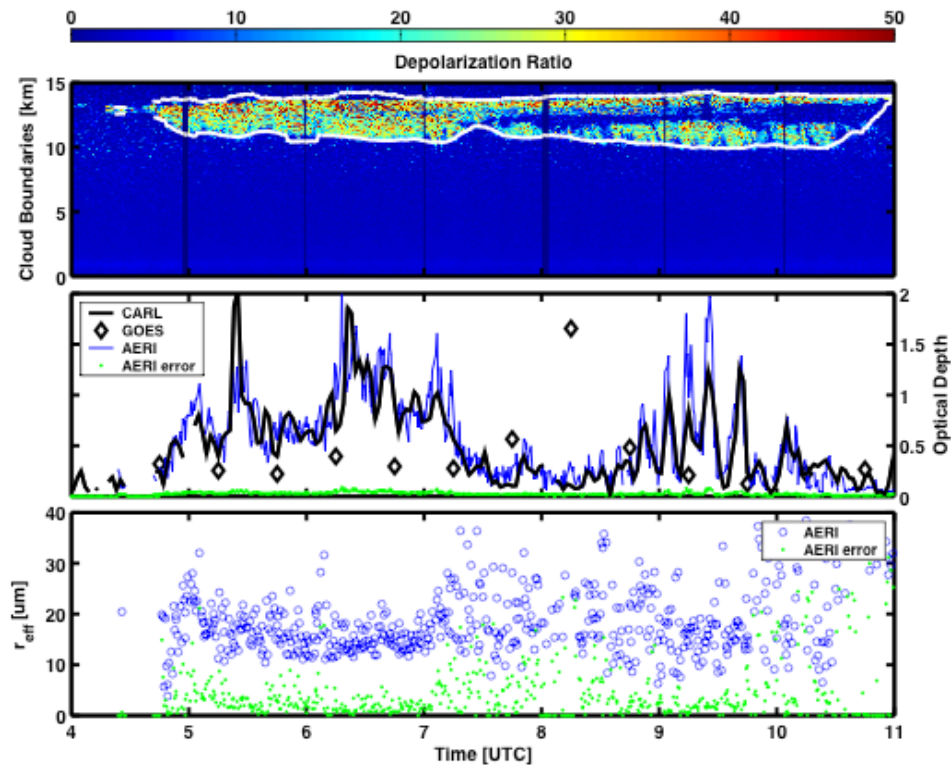


Figure 9. TX-2002 case from 29 November 2002. Top panel shows ARM SGP Raman lidar depolarization and cloud boundaries. Middle panel compares retrieved optical depths from the Raman lidar, AERI, and GOES-8. AERI retrieved cloud particle sizes are shown in the bottom panel.

The DeSlover AERI algorithm has also been applied to aircraft-based Scanning-HIS data. An aircraft sortie also occurred on 29 November 2002 and provided the opportunity to retrieve simultaneous above and below cloud optical properties as the aircraft flew over the SGP-CRF in four separate passes between 1600 and 1800 UTC. Figure 10, similar to Figure 9 but for 1400 through 2400 UTC, includes results from the aircraft measurements (red squares) for both cloud optical depth (middle panel) and bulk effective radius (bottom panel).

The ground-based AERI and aircraft-based Scanning-HIS cloud optical depth results agree to within a few percent. The optical depths from the Raman lidar are smaller than the HSR-IR optical depths because the Raman lidar data are attenuated before reaching cloud top. In this case, probably due to the larger cloud optical depth, the GOES-8 retrievals agree well with the AERI retrievals, despite the 4 km GOES field of view. The AERI cloud algorithm determines the cloud to be opaque near optical depths ~ 4 (e.g., 1800 to 2300 UTC). Local daytime occurred between 1400 and 2400 UTC, which allowed comparison between the IR retrievals and the daytime-only GOES-8 particle size retrievals (bottom panel). The ground-based AERI retrieved uncertainty in particle size decreases for optical depth > 1 and agrees well with both Scanning-HIS and GOES-8 results. The bulk effective radius increases as the cloud becomes geometrically thicker with decreasing cloud base. The retrieval of smaller particle sizes from the Scanning-HIS, compared with those from the AERI, is consistent with in situ measurements of ice crystal vertical profiles and gravitational settling of ice particles. The remote sensing retrieval of cloud properties from the ground-based AERI and airborne S-HIS instruments provides a key link to bridge the gap between the detailed measurements on the point scale to the cloud products derived from satellites.

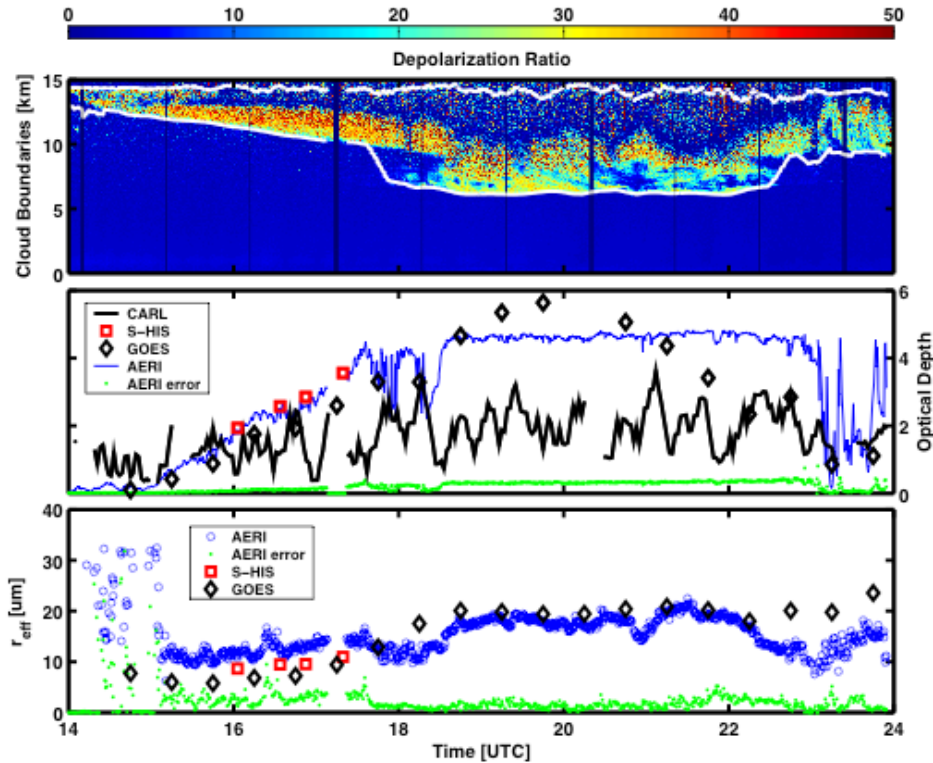


Figure 10. Similar to Figure 9, but 1400 to 2400 UTC. Data also includes aircraft-based Scanning-HIS optical depth (middle) and effective size (bottom) retrievals for simultaneous above cloud measurements of the cirrus, shown as red squares). The S-HIS and AERI derived optical depths are consistent with each other. However, the retrieved particle size is found to be about 20% smaller at cloud top by the S-HIS than the particle size at cloud bottom retrieved simultaneously from the ground-based AERI observations.

AERI data has also been used to classify Arctic clouds with optical depths less than 5 as water phase, ice phase, or mixed ice and water phase. This work was accomplished by Dave Turner as part of his doctoral dissertation at UW-Madison (Turner, 2003b; Turner et al., 2003c). The cloud phase determination algorithm takes advantage of the differing refractive indices of ice and water between 11 and 18 μm . Radiative transfer calculations are compared with AERI emissivity spectra to determine cloud phase. In cases of mixed phase clouds, the distribution of phases, in either adjacent layers or as a mixture within a layer, can usually be determined. The

Arctic cloud phase classification uses the AERI Extended Range (AERI-ER) system, with a longwave detector sensitivity between 5.5 and 25 μm .

Turner (2003b) and Turner et al. (2005) extended the Arctic cloud phase classification to cloud property retrievals. A physical retrieval based on an optimal estimation approach is used to retrieve cloud optical depth, ice fraction, liquid and ice water path, and the effective radius of the liquid water drops and ice crystals in mixed phase clouds from AERI-ER observations. Comparisons between calculations using the LBLDIS radiative transfer code and AERI observations are used to retrieve the cloud properties. LBLDIS was developed by David Turner and combines the LBLRTM and DISORT radiative transfer models into a single cloudy forward model. LBLDIS allows multiple cloud layers, high vertical resolution, and different crystal habits. HSR-IR radiances are calculated from atmospheric temperature and water vapor profiles, surface temperature, cloud layer boundaries, cloud habit, and cloud layer effective radius and optical depth.

Cloud microphysical properties were retrieved for 7 months during the SHEBA experiment between 1997 and 1998. The Turner algorithm found mixed-phase clouds 50% of the time, many of which had large infrared optical depths. The water droplet mode radius was found to be 10 μm in water clouds, and 7 μm in mixed phase clouds. The ice crystal effective radius was found to be smaller in mixed phase clouds than in ice clouds.

5.2 Cloud Radiative Transfer Closure Study at the ARM NSA Site

This section describes the preliminary results of a closure study undertaken to show how measurements from the ARM Barrow, Alaska site during MPACE can be used as input to state of the art cloudy radiative transfer models to reproduce the observations of upwelling infrared

radiance obtained by the Scanning-HIS (Holz et al. 2005). The Scanning-HIS offers a similar accuracy, resolution, and stability as the ground-based AERI, but from a mobile, airborne platform.

The data obtained during M-PACE are unique because they offer unprecedented measurements of Arctic clouds from an extensive aircraft and ground suite of *in situ* instruments, as well as active and passive remote sensing instrumentation. This study makes use of this extensive instrumentation network; especially, the University of Wisconsin Arctic High Spectral Resolution Lidar (AHSRL) in Barrow, AK, and the *in situ* cloud measurements from the Uni. of North Dakota Citation aircraft. The goal of this closure study is to use the unique AHSRL measurements of cloud optical depth, the ARM cloud radar information on particle size, observations of ice crystal shape from the Citation aircraft, and the airborne Scanning HIS observations of upwelling radiance above the cloud to make a quantitative assessment of the radiative transfer models used to compute infrared radiance in cloudy conditions. The relevance of this to our proposal is that these state-of-the-art cloudy radiative transfer models are being used to validate the cloud optical property representations used in satellite retrieval algorithms. See Section 3.1 of the proposal Narrative.

The forward calculations for the Scanning-HIS closure study use the cloudy radiative transfer algorithms described previously (the LBLDIS code developed by Dr. Dave Turner with cloud optical properties from the work by Dr. Ping Yang (Texas A&M)). The ground and aircraft measurements during M-PACE are used to constrain the LBLDIS input variables. Atmospheric state and surface temperature information are obtained from the NSA site radiosondes and down-looking infrared thermometer (IRT) temperatures, respectively. The AHSRL, deployed at the ARM NSA Barrow facility during M-PACE, provides vertically resolved cloud extinction

profiles and cloud depolarization. The AHSRL extinction measurements are integrated in the vertical and used to constrain the layer optical depths in the Scanning-HIS LBLDIS simulations. Combining the AHSRL data with that of the millimeter-wavelength cloud radar (MMCR), it is possible to retrieve vertical profiles of cloud effective radius (Eloranta et al. 2005). This retrieval is used to constrain the particle effective radius in the LBLDIS simulations. *In situ* aircraft measurements of ice crystal size distributions and crystal habits compliment the lidar-radar effective radius retrievals.

An M-PACE case on 17 October 2004 demonstrates the value of combining ARM data with these additional observations to validate cloudy radiative transfer models. Figure 11 shows the AHSRL cloud aerosol backscatter cross-section (top) and depolarization (center) for the latter part of the day. The cirrus cloud is optically thin, with AHSRL determined cloud optical depth ranging between 0.2 and 2.0, but the geometric thickness is greater than 5 km during most of the time period. Based on Cloud Particle Imager measurements, we know the cloud is primarily composed of bullet rosettes. To characterize the vertical structure of the cloud in the LBLDIS simulations, we divide the cloud into 5 layers, marked by the white lines in Figure 5. A mean

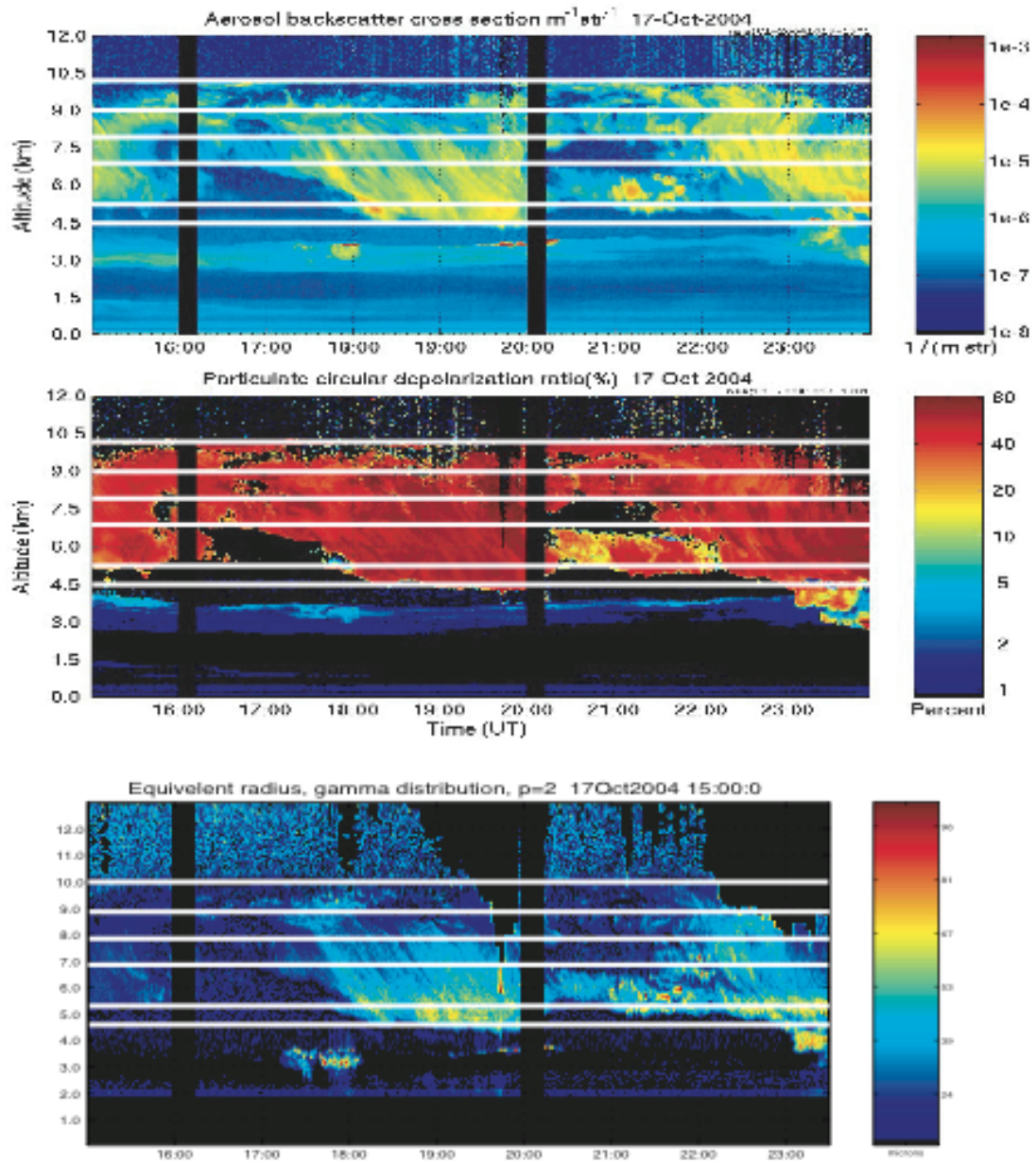


Figure 11. The AHSRL cloud aerosol backscatter cross-section (top), depolarization (center), and combined AHSRL-MMCR cloud effective radius (bottom) are presented between 1500 and 2359 UTC on 17 October 2004 at the NSA ARM site during M-PACE. White lines show the cloud layer boundaries used in the LBLDIS simulations.

effective radius and optical depth for each simulation layer is chosen from consideration of the AHSRL integrated optical depth and AHSRL-MMCR effective radius profile. These layer cloud properties, calculated for two minute averages of AHSRL and MMCR data, along with

atmospheric absorptions calculated from ARM radiosonde profiles are used in LBLDIS to simulate HSR-IR radiances.

The five HSR-IR simulations closest to the 2109 UTC Scanning-HIS overpass of the NSA site are shown in Figure 12. The AHSRL aerosol back-scatter cross-section measurements in Figure 5 show a considerable amount of cloud structure variability, which in turn is translated to variability in the simulated upwelling IR radiances. The black line in Figure 12 shows that the measured Scanning-HIS radiance at 2109 UTC most closely matches the 2101 UTC simulation. The brightness temperature differences between the simulated and measured Scanning-HIS spectra are presented in the right half of Figure 6. The simulated minus measured differences are less than a degree on both sides of the ozone absorption ($750 - 1000 \text{ cm}^{-1}$ and $1100 - 1200 \text{ cm}^{-1}$) for the best fit case. This demonstrates that AHSRL extinction profiles correlate closely with the infrared optical depths and are capable of representing the infrared extinction profile assuming a relationship of unity between the infrared and visible extinction efficiency. The slope of the Scanning-HIS simulated brightness temperature spectrum between $750 - 900 \text{ cm}^{-1}$ shows a sensitivity to cloud particle size and ice crystal habit. The reasonable match between the simulated spectra using the AHSRL-MMCR effective radius retrieval and the measured radiances is encouraging, but further research is needed to understand better the relationship between the AHSRL-MMCR derived cloud particle size profile and retrieved effective radius in the infrared. Case studies like the one described previously will be used to quantify the errors in retrieval of cloud properties from ground-based ARM data and from satellite observations over the ARM sites, the products of which are used by ARM focus groups such as the BBHRP.

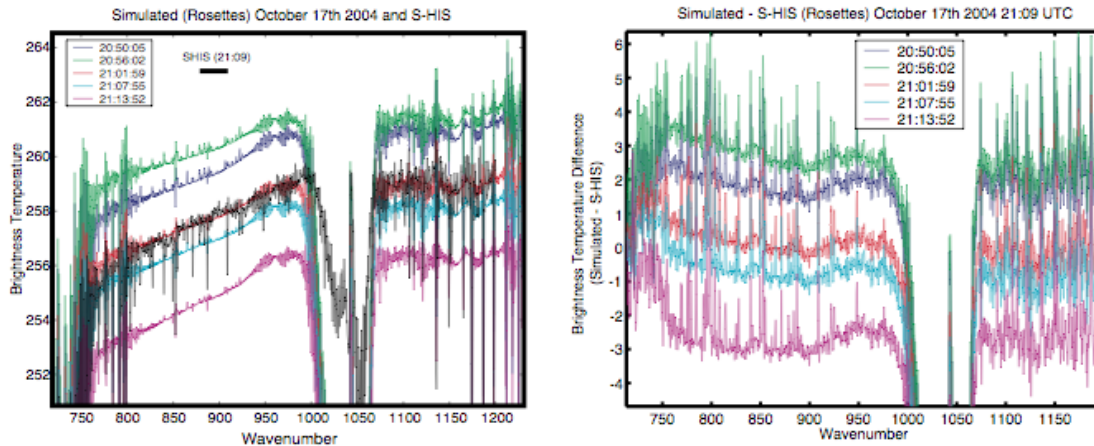


Figure 12. Simulated cloudy radiances using the AHSRL and MMCR retrieved cloud optical thickness and effective radius and measured Scanning-HIS radiances at 2109 UTC are shown to the left. The differences between measured Scanning-HIS brightness temperatures and the simulations are shown to the right.

5.3. AIRS Cloud Property Retrievals

The Atmospheric Infrared Sounder (AIRS) aboard the NASA Aqua platform ushered in a new era of space-borne high spectral resolution infrared measurements. These data, along with IASI data on the METOP-A platform and CrIS on the NPP and NPOESS platforms, have the potential to greatly benefit ARM and the climate monitoring communities. The development of the UW-Madison AIRS cloud property retrieval algorithm has been supported by a combination of NAVY, NOAA, and NASA projects with Dr. Jun Li as lead investigator, but the application of the UW AIRS algorithm to the MPACE intensive operating period over the North Slope of Alaska has been supported by this grant. AIRS retrieval products include cloud microphysical properties such as optical depth at $0.55 \mu\text{m}$ and effective particle size, as well as cloud top pressure and cloud effective emissivity, for both daytime and nighttime AIRS data.

AIRS radiance observations in the region between $720 - 790 \text{ cm}^{-1}$ have strong CO_2 absorption and provide high vertical resolution weighting function peaks at different atmospheric

levels. It provides cloud top height with significantly higher accuracy than MODIS, with an improvement of 20 to 30 hPa in cloud top pressure (Li et al. 2004b). The AIRS cloud property retrieval algorithms developed at the University of Wisconsin make use of the higher spatial resolution of the MODIS instrument for cloud clearing and cloud classification. Collocated MODIS data are used to characterize cloud variability within the larger AIRS footprint (Li et al. 2004a). For example, the collocated MODIS 1 km cloud phase product is used to determine if an AIRS footprint contains water clouds, ice clouds, or mixed phase clouds, and the MODIS cloud classification developed by Li et al. (2003) is used to determine if an AIRS footprint is partly cloudy or overcast, as well as if the clouds are within a single layer or in multiple layers. Cloud top pressure and emissivity are determined using AIRS channels between 720 and 790 cm^{-1} (Li et al. 2004b).

The minimum residual approach developed by Li et al. (2005) is used to retrieve cloud optical properties once the cloud top pressure and effective emissivity are known. The minimum residual approach involves minimizing the differences between AIRS observations and radiative transfer calculations between 790 and 1130 cm^{-1} . The radiative transfer calculations are performed using a cloudy fast model. In the fast model, ice cloud single-scattering properties are crystal habit and size dependent. Aggregates are used for large particles over 300 μm in maximum dimension, various hexagonal geometries for particles between 50 and 300 μm , and particles under 50 μm are assumed to be droxtals (Wei et al. 2004). Water cloud single scattering properties are calculated from classical Lorenz-Mie theory. Examples of the AIRS cloud property retrievals are shown for a case on 17 October 2004 during M-PACE (see also Huang et al., 2005). The 2200 UTC AIRS 11 μm (channel 769) brightness temperature and the retrieved

cloud top height can be seen in Figure 13. The ARM NSA Barrow site is at the center of the red box in each image.

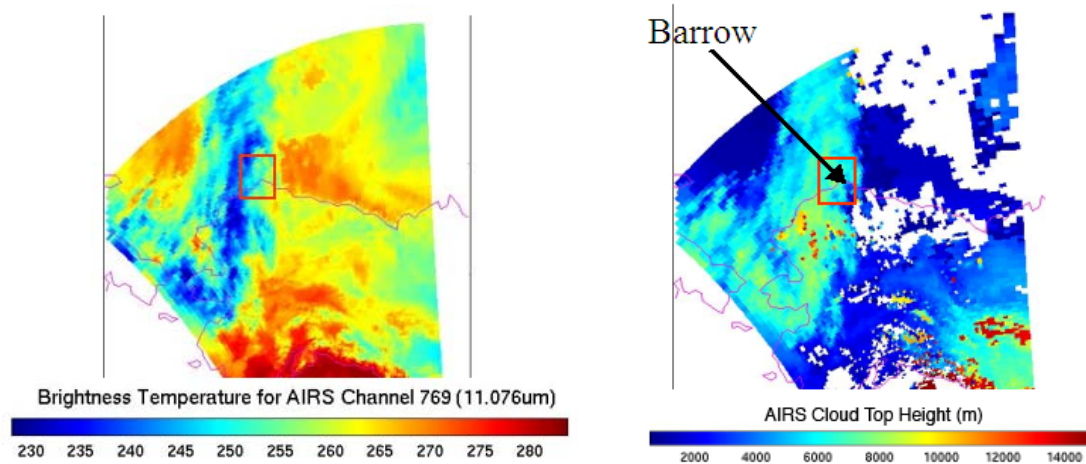


Figure 13. AIRS 11 μm (Channel 769) brightness temperature (left panel) for 2220 UTC on 17 October 2004. The ARM NSA Barrow is located at the center of the red box in each image. The right panel shows the AIRS derived cloud-top height.

Figure 14 compares the aerosol backscatter cross section from the AHSRL with AIRS retrieved cloud top height at the time of the Barrow overpass. The cloud top height from the operational MODIS product also shown. Figure 9 compares the AIRS longwave observations (black line), with clear-sky calculations based on an ECMWF forecast (blue line), and the cloudy calculations based on the retrieved AIRS cloud-top pressure of 407.47 hPa, cloud particle diameter of 33.51 μm , and cloud optical thickness of 1.44 at Barrow.

It should be noted that AIRS is able to provide cloud microphysical information during both the daytime and nighttime, while the operational MODIS cloud microphysical properties are only available during daytime with solar zenith angle less than 80 degree. For the M-PACE

case presented here (Figures 14 and 15), no MODIS particle size or optical thickness retrievals are available over the NSA Barrow site due to the large solar zenith angle.

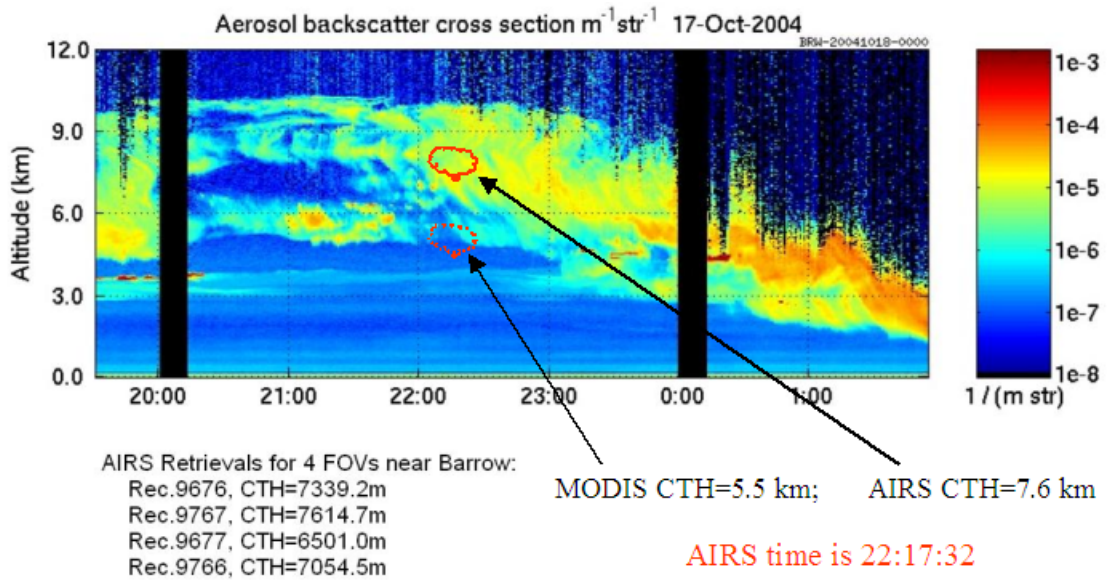


Figure 14. The AIRS retrieved cloud top height is overlaid on the AHSRL aerosol backscatter cross section from 17 October. For reference, the cloud top height from the operational MODIS product is also shown.

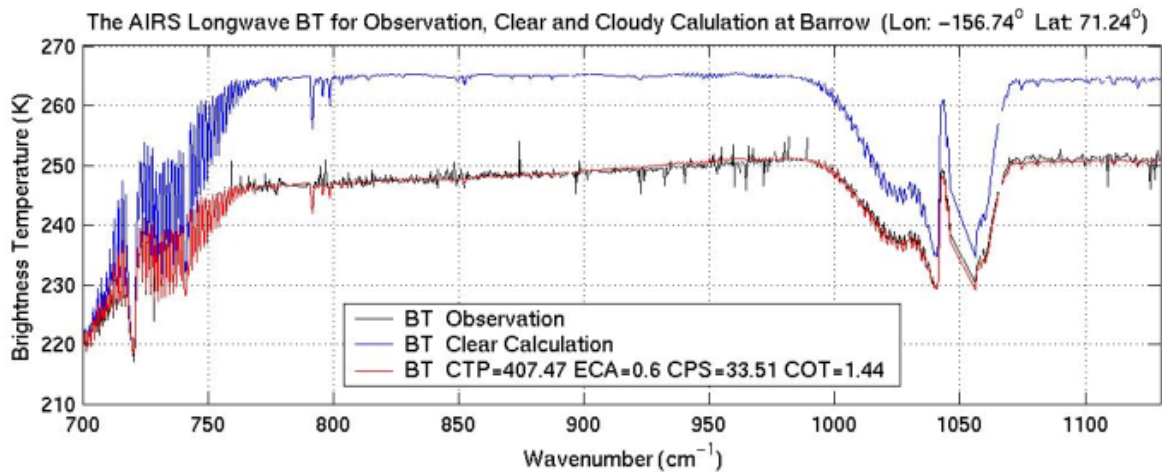


Figure 15. Modeled clear sky calculations based on an ECMWF forecast are shown in blue and AIRS observations are shown in black. The red line is for a simulated cloudy atmosphere, based on AIRS retrievals over the NSA site, with a cloud-top pressure of 407.5 hPa, a cloud particle diameter of 33.5 μm , and a cloud optical thickness of 1.44.

6. AERI Science Quality Assessment

Achievements regarding AERI data science quality assessment under the current funding include:

- The characterization of rapid sample AERI data
- The development and characterization of an AERI Principle Component Noise Filter (Turner et al., 2006).
- AERI processing software refinements, as described below.

An example of recent work under this grant regarding AERI data science quality assessment involved the detailed investigation and correction of a software problem that showed up when the ER-AERI instruments in Barrow, Alaska was switched from normal sampling mode (10 minute) to rapid sampling (10 second) with a corresponding increase in random measurement noise on each individual spectrum. The move to rapid sampling was motivated by a scientific desire to increase the frequency of sky sampling in order to better match the AERI data in time with other sensors such as the microwave radiometer as well as to provide a more continuous sampling of cloud edge effects. However, it was assumed that the average of the relatively noisy rapid sample calibrated radiance spectra would equal the original normal sampling with longer dwell times for uniform sky conditions. In practice it was discovered that the software was applying a non-symmetric noise trap which was not apparent on an individual sample but was evident in a large statistical set. Figure 16 shows the result of averaging a 12 hour period of ER-AERI data using both the original AERI calibration software and a modified version of the software which performs a symmetric noise test, the corrected software has been documented and made available to the ARM program for incorporation into the ARM facility instruments. Reprocessing of AERI data in the ARM archive to correct for this error is under discussion and will likely be combined with some other calibration related improvements.

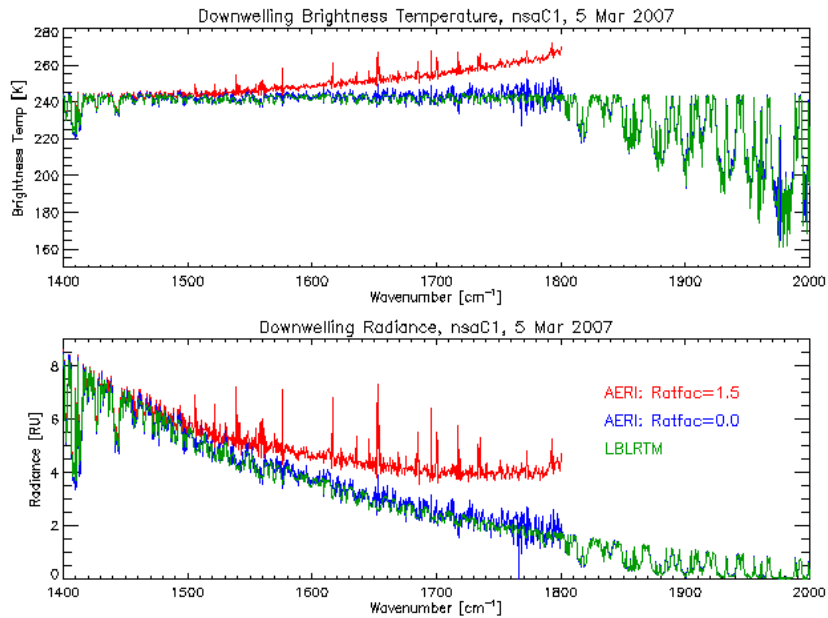


Fig 16: Mean radiance from the NSA C1 AERI system from 00:00-12:00 UTC on 5 March 2007, with the RATFAC test turned on (red) and the RATFAC test disabled (blue). Channel 1 AERI data range from 400-1800 cm^{-1} , whereas channel 2 AERI data range from 1800 – 3020 cm^{-1} ; however, the channel 2 AERI data are virtually identical for the two datasets in the 1800-2000 cm^{-1} region shown. The LBLRTM calculation for the radiosonde launched at 05:30 UTC is also shown (green). The AERI software was modified to correct this error.

7. References and Bibliography

- Aumann, H. H., M. T. Chahine, C. Gautier, M. D. Goldberg, E. Kalnay, L. M. McMillin, H. E. Revercomb, P. W. Rosenkranz, W. L. Smith, D. H. Staelin, L. L. Strow, and J. Susskind, AIRS/AMSU/HSB on the Aqua Mission: Design, Science Objectives, Data Products, and Processing Systems, 2003: IEEE Transactions on Geoscience and Remote Sensing, **41**, 253-264.
- Borg, L., D. Tobin, D. Turner, R. Holz, D. DeSlover, E. Eloranta, R. Knuteson, H. Revercomb, L. Moy, 2008a: Assessing the Vertical Structure of Radiative Heating Using Radar/Lidar/AERI for Cirrus Cloud Events at SGP. *Proc. 18th ARM Science Team Meeting*, March 10-14, Norfolk, VA.

- Borg, L., D. Turner, R. Holz, D. Tobin, H. Revercomb, Improving Cirrus Cloud Characterization with Raman Lidar Measurements at Southern Great Plains, to be submitted to Geophysical Letters, 2008b.
- Clough, S., M. Shepard, E. Mlawer, J. Delamere, K. Cady-Pereira, D. Tobin, H. Revercomb, R. Knuteson, D. Turner. ARM Radiative Transfer Modeling and Remote Sensing. *Proc. 15th ARM Science Team Meeting*, March 14-18, Daytona Beach, FL.
- Clough, S. A., M. W. Shepard, E. Mlawer, J. S. Delamere, M. Iacono, K. Cady-Pereira, S. Boukabara, and P. D. Brown, 2005: Atmospheric radiative transfer modeling: a summary of the AER codes. *J. Quant. Spectrosc. Radiat. Transfer*, **91**, 233-244.
- Collard, A. D., S. A. Ackerman, W.L. Smith, X. Ma, H. E. Revercomb, R. O. Knuteson, and S.-C. Lee, 1995: Cirrus cloud properties derived from high spectral resolution infrared spectrometry during FIRE II. Part II: Ground-based HIS results. *J. Atmos. Sci.*, **52**, 4264-4275.
- Dedecker, R., Knuteson, R., Revercomb, H., Tobin, D., Ciganovich, N., Dirx, T., Feltz, W., Garcia, R., Hackel, D., Holz, R., and Turner, D., 2005: New AERI Deployments and the Status of AERI Engineering Changes. *Proc. 15th ARM Science Team Meeting*, March 14-18, Daytona Beach, FL.
- Dedecker, R., J. Demirgian, R. Knuteson, H. Revercomb, D. Tobin, D. Turner, 2006: The ARM Atmospheric Emitted Radiance Interferometer (AERI): Status and Preliminary Assessments of Instrument Deployments in 2006. *Proc. 16th ARM Science Team Meeting*, March 27-31, Albuquerque, NM.
- DeSlover, D.H., W.L. Smith, P.K. Piironen, E.W. Eloranta, 1999: A methodology for measure cirrus cloud visible-to-infrared spectral optical depth ratios, *J. Atmos. Oceanic Tech.*, **16**, pp.251-262. DeSlover, D., R. Holz, D. Turner, H. Revercomb, 2006: Aircraft S-HIS Observations during MPACE. *Proc. 16th ARM Science Team Meeting*, March 27-31, Albuquerque, NM.

- DeSlover, D., R. Holz, D. Turner, H. Revercomb, 2006: Aircraft S-HIS Observations during MPACE. *Proc. 16th ARM Science Team Meeting*, March 27-31, Albuquerque, NM.
- Donovan, D. P., and A. C. A. P. van Lammeren (2001a), Cloud effective particle size and water content profile retrievals using combined lidar and radar observations 1. Theory and examples, *J. Geophys. Res.*, *106*(D21), 27,425–27,448.
- Donovan, D. P., A. C. A. P. van Lammeren, R. J. Hogan, H. W. J. Russchenberg, A. Apituley, P. Francis, J. Testud, J. Pelon, M. Quante, and J. Goddard (2001b), Cloud effective particle size and water content profile retrievals using combined lidar and radar observations 2. Comparison with IR radiometer and in situ measurements of ice clouds, *J. Geophys. Res.*, *106*(D21), 27,449–27,464.
- Dykema, J.A., S.S. Leroy, B.F. Farrell, J.G. Anderson, D. Tobin, H. Revercomb, X. Huang, 2005: Confronting Models with Atmospheric Radiation Measurement Data: A statistical comparison of Southern Great Plains Atmospheric Emitted Radiance Interferometer Radiance Spectra and Global Climate Models Output. *Proc. 15th ARM Science Team Meeting*, March 14-18, Daytona Beach, FL.
- Dykema, J., S. Leroy, J. Anderson, D. Tobin, R. Knuteson, H. Revercomb, 2006: Time series analysis of AERI radiances for GCM testing and improvement. *Proc. 16th ARM Science Team Meeting*, March 27-31, Albuquerque, NM.
- Ebert, Elizabeth E., and Judith A. Curry, A parameterization of ice cloud optical properties for climate models, *J. Geophys. Res.*, *97*, D4, 3831-3836, March 20, 1992.
- Eloranta, E.W., 2005: University of Wisconsin High Spectral Resolution Lidar operations during MPACE. *Proc. 15th ARM Science Team Meeting*, March 14-18, Daytona Beach, FL.
- Feltz, W., B. Howell, D. Turner, R. Mahon, R. Knuteson, 2005: AERI Thermodynamic Profiling VAP Improvements and Status. *Proc. 15th ARM Science Team Meeting*, March 14-18, Daytona Beach, FL.
- Ferrare, R. A., E.V. Browell, S. Ismail, S. Kooi, L.H. Brasseur, V.G. Brackett, M. Clayton, J. Barrick, G.

- Diskin, J. Goldsmith, B. Lesht, J. Podolske, G. Sachse, F.J. Schmidlin, D. Turner, D. Whiteman, D. Tobin, L. Miloshevich, 2004: Characterization of upper troposphere water vapor measurements during AFWEX using LASE. *J. Atmos. Oceanic Tech.*, 21, 1790-1808.
- Geier, E. B., R. N. Green, D. P. Kratz, P. Minnis, W. F. Miller, S. K. Nolan, and C. B. Franklin, 2003: Clouds and the Earth's Radiant Energy System (CERES) Data Management System Single Satellite Footprint TOA/Surface Fluxes and Clouds (SSF) Collection Document.
- Holz, R., DeSlover, D., Revercomb, H., Tobin, D., Knuteson, R., Turner, D., and Eloranta, E., 2005: Validation of Infrared Cloud Radiative Transfer Simulations and Spectral Cloud Properties Retrievals Using S-HIS, AERI and HSRL Measurements from M-PACE. *Proc. 15th ARM Science Team Meeting*, March 14-18, Daytona Beach, FL.
- Huang, A., Li, J., Baggett, K., Wu, X., Revercomb, H., Tobin, D., and Knuteson, R.: 2005. Cloud Property Retrievals Using AIRS Data During M-PACE. *Proc. 15th ARM Science Team Meeting*, March 14-18, Daytona Beach, FL.
- IPCC, 2007: Climate Change 2007: The Physical Science Basis. Contribution of Working Group I to the Fourth Assessment Report of the Intergovernmental Panel on Climate Change [Solomon, S., D. Qin, M. Manning, Z. Chen, M. Marquis, K.B. Averyt, M. Tignor and H.L. Miller (eds.)]. Cambridge University Press, Cambridge, United Kingdom and New York, NY, USA, pp. 996.
- Knuteson R. O., H. E. Revercomb, F. A. Best, N. C. Ciganovich, R. G. Dedecker, T. P. Dirks, S. C. Ellington, W. F. Feltz, R. K. Garcia, H. B. Howell, W. L. Smith, J. F. Short, D. C. Tobin, 2004a: Atmospheric Emitted Radiance Interferometer (AERI) Part I: Instrument Design, *Journal of Atmospheric and Oceanic Technology*, Volume 21 (2004), Issue 12, pp. 1763-1776.
- Knuteson R. O., H. E. Revercomb, F. A. Best, N. C. Ciganovich, R. G. Dedecker, T. P. Dirks, S. C. Ellington, W. F. Feltz, R. K. Garcia, H. B. Howell, W. L. Smith, J. F. Short, D. C. Tobin, 2004b: Atmospheric Emitted Radiance Interferometer (AERI) Part II: Instrument

Performance, *Journal of Atmospheric and Oceanic Technology*, Volume 21 (2004), Issue 12, 1777-1789.

Knuteson, R., W. Felz, H. Revercomb, D. Tobin, 2005: Seasonal Dependence of the Infrared Land Surface Emissivity in the Vicinity of the ARM SGP Central Facility. *Proc. 15th ARM Science Team Meeting*, March 14-18, Daytona Beach, FL.

Li, J., H.-L. Huang, C.-Y. Liu, P. Yang, T. J. Schmit et al., 2005: Retrieval of cloud microphysical properties from MODIS and AIRS. *J. Appl. Meteorol.*, **44**, 10, DOI: 10.1175/JAM2281.1

Li, J., W. P. Menzel, F. Sun, T. J. Schmit, and J. Gurka, 2004a: AIRS sub-pixel cloud characterization using MODIS cloud products, *J. Appl. Meteorol.* **43**, No.8, 1083 – 1094.

Li, J., W. P. Menzel, W. Zhang, F. Sun, T. J. Schmit, J. Gurka, and E. Weisz, 2004b: Synergistic use of MODIS and AIRS in a variational retrieval of cloud parameters, *J. Appl. Meteorol.*, **43**, 1619 - 1634.

Li, J., W. P. Menzel, Z. Yang, R. A. Frey, and S. A. Ackerman, 2003: High spatial resolution surface and cloud type classification from MODIS multi-spectral band measurements, *J. Appl. Meteorol.*, **42**, 204 – 226.

Loeb, N. G., S. Kato, K. Loukachine, and N. Manalo-Smith, 2005: Angular distribution models for top-of-atmosphere radiative flux estimation from the Clouds and the Earth's Radiant Energy System instrument on the Terra satellite. Part I: Methodology. *J. Atmos. Ocean. Technol.*, **22**, 338-351.

Mace, GG, TP Ackerman, P Minnis, and DF Young. 1998. "Cirrus Layer Microphysical Properties Derived from Surface-Based Millimeter Radar and Infrared Interferometer Data." *J. Geophys. Res.* **103**: 23207-16.

Minnis, P., A. V. Gambheer, and D. R. Doelling, 2004: Azimuthal anisotropy of longwave and infrared window radiances from the Clouds and the Earth's Radiant Energy System on the

- Tropical Rainfall Measuring Mission and Terra satellites. *Journal of Geophysical Research-Atmospheres*, **109**, D08202.
- Minnis, P., and M. M. Khaiyer, 2000: Anisotropy of land surface skin temperature derived from satellite data. *J. Appl. Meteorol.*, **39**, 1117-1129.
- Moy, L., H.E. Revercomb, R.O. Knuteson, D.D. Turner, E. Kassianov, 2005: Retrieving Aerosols from the Atmospheric Emitted Radiance Interferometer: Can it be Done? *Proc. 15th ARM Science Team Meeting*, March 14-18, Daytona Beach, FL.
- Moy, L., D.D. Turner, E. Kassianov, W.P. Arnott, 2006: Retrieving the relative number of fine to coarse mode aerosol from ground-based visible and infrared observation. *Proc. 16th ARM Science Team Meeting*, March 27-31, Albuquerque, NM.
- Moy, L., H. Revercomb, D. Tobin, L. Borg, R. Knuteson, J. Li, D. Turner, 2008a: Clear- and All-sky TOA OLR Comparisons Between RTM Calculations and CERES Observations. *Proc. 18th ARM Science Team Meeting*, March 10-14, Norfolk, VA.
- Moy, L., R. Knuteson, D. Tobin, H. Revercomb, L. Borg, J. Susskind, Assessing Clear Sky OLR with CERES and AIRS, to be submitted to *JGR-Atmospheres*, 2008b.
- Revercomb, H. E., D. D. Turner, D. C. Tobin, R. O. Knuteson, W. F. Feltz, J. Barnard, J. Bosenberg, S. Clough, D. Cook, R. Ferrare, J. Goldsmith, S. Gutman, R. Halthore, B. Lesht, J. Liljegren, H. Linné, J. Michalsky, V. Morris, W. Porch, S. Richardson, B. Schmid, M. Splitt, T. Van Hove, E. Westwater, and D. Whiteman, 2003: The ARM Program's Water Vapor Intensive Observation Periods: Overview, Initial Accomplishments, and Future Challenges, *Bull. Amer. Meteor. Soc.*, **84**, p. 217–236.
- Revercomb, H., Tobin, D., Knuteson, R., Best, F., Laporte, D., Ellington, S., Werner, M., Dedecker, R., Garcia, R., Ciganovich, N., Howell, B., Dutcher, S., Taylor, J., Huang, H., Li, J., and Holz, R., 2005: Scanning High-Resolution Interferometer Sounder (S-HIS) Participation in the Mixed-Phase Arctic Cloud Experiment (M-PACE) on the ARM-UAV Proteus Aircraft, *Proc. 15th ARM Science Team Meeting*, March 14-18, Daytona Beach, FL.

- Revercomb, H., D. DeSlover, R. Holz, R. Knuteson, J. Li, L. Moy, D. Tobin, D. Turner, 2006: BBHRP Assessment Using Ground and Satellite-based High Spectral Resolution Infrared Observations. *Proc. 16th ARM Science Team Meeting*, March 27-31, Albuquerque, NM.
- Revercomb, H., R. Holz, R. Knuteson, L. Moy, D. Tobin, D. Turner, 2007: BBHRP Assessment Using Ground Measurements and Satellite-based High Spectral Resolution Infrared Observations in Clear Sky Conditions. *Proc. 17th ARM Science Team Meeting*, March 26-30, Monterey, CA.
- Tobin, D.C., F.A. Best, P.D. Brown, S.A. Clough, R.G. Dedecker, R.G. Ellingson, R.K. Garcia, H.B. Howell, R.O. Knuteson, E.J. Mlawer, H.E. Revercomb, J.F. Short, P.F.W. van Delst, V.P. Walden, 1999: Downwelling spectral radiance observations at the SHEBA ice station: water vapor continuum measurements from 17 to 26 μm . *J. Geophys. Res.*, Vol. 104, no. D2, pp. 2081-2092.
- Tobin, D. C., H. E. Revercomb, D. D. Turner, 2002b: Overview of the ARM/FIRE Water Vapor Experiment (AFWEX), *Proc. Twelfth ARM Science Team Meeting*, St. Petersburg, FL, 8-12 April 2002.
- Tobin, David C.; Revercomb, HE.; Knuteson, RO.; Best, FA.; Smith, WL.; Ciganovich, N.; Dedecker, G.; Dutcher, S; Ellington, SD.; Garcia, RK.; Howell, H. B; LaPorte, Daniel D.; Mango, SA.; Pagano, TS.; Taylor, JK.; van Delst, P; Vinson, KH. and Werner, MW.. Radiometric and spectral validation of Atmospheric Infrared Sounder observations with the aircraft-based Scanning High-Resolution Interferometer Sounder. *Journal of Geophysical Research*, Volume 111, 2006, Doi:10.1029/2005JD006094, 2006.
- Tobin, D., H. Revercomb, R. Knuteson, W. Feltz, L. Moy, B. Lesht, T. Cress, L. Strow, S. Hannon, E. Fetzer, 2005: ARM Site Atmospheric State Best Estimates for AIRS Forward Model and Retrieval Validation. *Proc. 15th ARM Science Team Meeting*, March 14-18, Daytona Beach, FL.
- Tobin D. C., H. E. Revercomb, R. O. Knuteson, B. M. Lesht, L. L. Strow, S. E. Hannon, W. F. Feltz, L. A. Moy, E. J. Fetzer, T. S. Cress (2006), Atmospheric Radiation Measurement site

- atmospheric state best estimates for Atmospheric Infrared Sounder temperature and water vapor retrieval validation, *J. Geophys. Res.*, 111, D09S14, doi:10.1029/2005JD006103.
- Tobin, D. C. and Coauthors, 2006: Atmospheric Radiation Measurement site atmospheric state best estimates for Atmospheric Infrared Sounder temperature and water vapor retrieval validation. *Journal of Geophysical Research-Atmospheres*, **111**, D09S14.
- Tobin, D., D. Turner, L. Borg, R. Holz, L. Moy, H. Revercomb, R. Knuteson, 2007: Cirrus Cloud Flux Study Using Lidar/Radar/AERI Derived Cloud Properties. *Proc. 17th ARM Science Team Meeting*, March 26-30, Monterey, CA.
- Turner, D. D., B. M. Lesht, S. A. Clough, J. C. Liljegren, H. E. Revercomb, and D. C. Tobin, 2003a: Dry bias and variability in Vaisala RS80-H Radiosondes: The ARM experience. *J. Atmos. and Ocean. Tech.*, 20, 117– 132.
- Turner, D.D., S.A. Ackerman, B.A. Baum, H.E. Revercomb, and P. Yang, 2003b: Cloud phase determination using ground-based AERI observations at SHEBA. *J. Appl. Meteor.*, 42, p. 701-715.
- Turner, D. D., D. C. Tobin, S. A. Clough, P. D. Brown, R. G. Ellingson, E. J. Mlawer, R. O. Knuteson, H. E. Revercomb, T. J. Shippert, W. L. Smith, 2004: The AERI LBLRTM QME: A closure experiment for downwelling high spectral resolution infrared radiance, *J. Atmos. Sci.*, **61**, 2657-2675.
- Turner, D.D., 2005: Artic mixed-phase cloud properties from AERI lidar observations: Algorithm and results from SHEBA. *J. Appl. Meteor.*, 44, p. 427-444.
- Turner, D., C. Lo, R. Knuteson, 2005: A Principal Component Analysis Noise Filter VAP to Remove Uncorrelated Noise from AERI Observations. *Proc. 15th ARM Science Team Meeting*, March 14-18, Daytona Beach, FL.
- Turner, D.D., R.O. Knuteson, H.E. Revercomb, C. Lo, and R.G. Dedecker, 2006: Noise reduction of Atmospheric Emitted Radiance Interferometer (AERI) observations using principal component analysis. *J. Atmos. Oceanic Technol.*, 23, 1223-1238.

Wei, H., P. Yang, J. Li, B. A. Baum, H. L. Huang, S. Platnick, and Y. X. Hu, 2004: Retrieval of ice cloud optical thickness from Atmospheric Infrared Sounder (AIRS) measurements, *IEEE Trans. on Geosci. and Remote Sensing*, 42, 2254 - 2267.